Volume 1

IV. USGS Research

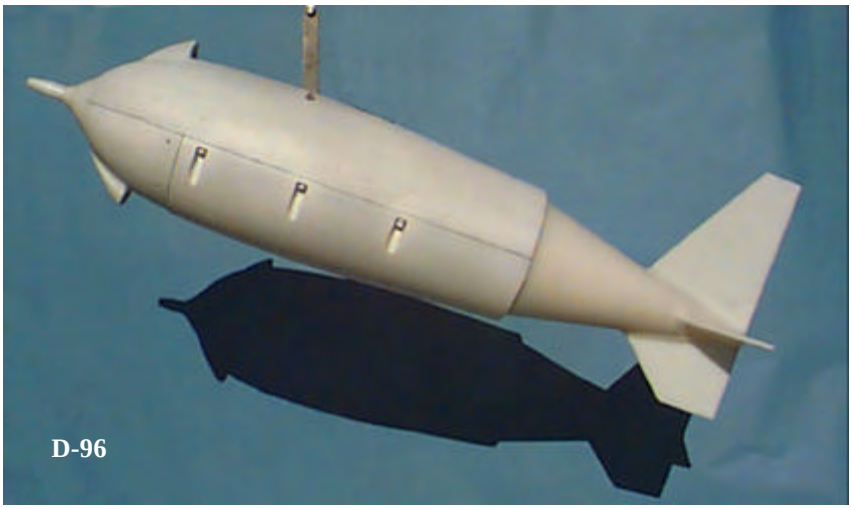

IV. USGS Research

TABLE OF CONTENTS

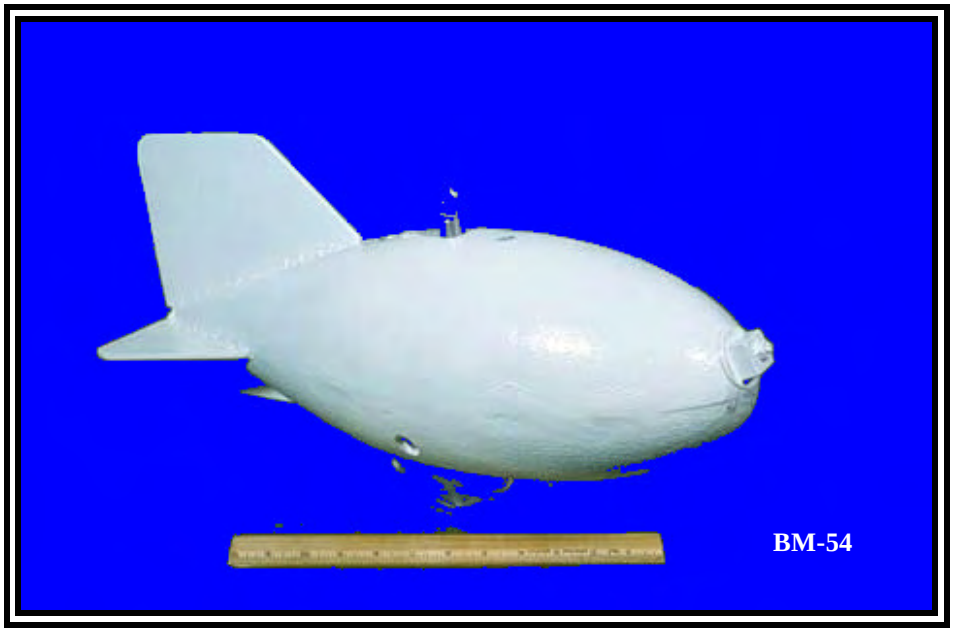

MECHANICS OF DEBRIS FLOWS AND DEBRIS-LADEN FLASH FLOODS

By Richard M. Iverson, Hydrologist, USGS, Vancouver, Washington;
Roger P. Denlinger, Geophysicist, USGS, Vancouver, Washington

Abstract: A new mathematical model developed to predict behavior of debris flows and avalanches also holds promise for predicting behavior of debris-laden flash floods. The model assumes that debris flows behave as mixtures of interacting Newtonian fluids and Coulomb solids. Solid and fluid constituents obey three-dimensional mass and momentum balances, which are summed and depth-integrated to yield equations that describe shallow flows of the mixture as a whole. An important distinction between these mixture equations and standard shallow-water equations results from strong variation of flow resistance due to interacting solid and fluid forces. Partitioning of flow resistance between solid and fluid components depends on fluid pressure, which evolves as flow evolves. If fluid pressure supports the total weight of the flowing mass, all resistance results from hydrodynamic forces, and the equations reduce to the conventional shallow-water form. If fluid pressure supports none of the weight of the flowing mass, all flow resistance results from Coulomb friction between interacting solids, and the equations describe motion of granular avalanches. A combination of solid and fluid resistance typifies debris flows and debris-laden flash floods. In these flows solid resistance commonly is concentrated at the fronts of advancing bores that may be heavily freighted with rocks and woody debris. Riemann methods provide an effective tool for solving the shallow flow equations numerically and predicting unsteady motion of debris flows and flash floods along paths with arbitrary geometry and inclination.

INTRODUCTION

Debris flows are churning, water-saturated masses of fine sediment, rocks, and assorted detritus that originate on mountain slopes and course down stream channels when they reach valley floors. Strong interactions of solid and fluid forces greatly influence the behavior of debris flows and distinguish them from related phenomena such as rock avalanches and water floods (Iverson, 1997). However, flash floods can resemble debris flows if floods entrain enough woody debris or coarse sediment to markedly increase friction at the fronts of advancing bores.

Mechanistic modeling of debris flows and debris-laden flash floods traditionally entails fitting model predictions to field data by adjusting the values of flow-resistance coefficients. Uncertainties about flow rheology and resistance afford great latitude for adjusting coefficient values until desirable fits are attained. However, coefficient adjustment lends little mechanical insight and provides no foundation for development of improved theoretical models.

In this paper we describe a depth-averaged flow model that avoids use of adjustable coefficients in most circumstances. The model was originally developed to simulate debris flows but is readily adaptable to simulation of debris-laden flash floods. For debris-flow simulations, flow resistance is computed from the following quantities: flow-path topography represented by gridded elevation data, sub-grid-scale bed topography (roughness) represented by a Coulomb friction angle, the internal Coulomb friction angle of the granular solids, the pore-pressure diffusivity of the solid-fluid mixture,

and the viscosity and volume fraction of the fluid phase. For flood calculations viscous fluid resistance must be replaced by an expression that accounts for hydrodynamic turbulence. In all cases the model accounts for the strong influence of cross-stream momentum fluxes on flow dynamics, because it computes motion of debris flows or debris-laden floods across three-dimensional terrain.

GOVERNING EQUATIONS

We first summarize the depth-averaged equations of motion we use to simulate debris flows. Elsewhere we provide detailed derivations of these equations (Iverson and Denlinger, 2000; Denlinger and Iverson, 2000). The equations express the laws of conservation of mass and linear momentum for concentrated mixtures of Coulomb granular solids and Newtonian viscous liquids without significant fluid turbulence. The equations are referenced to a local coordinate system that is fitted to the underlying topography (Figure 1). For each local coordinate system (i.e. each cell or facet of topography) the equations may be written compactly as

$$\frac{\partial \mathbf{U}}{\partial t} + \frac{\partial \mathbf{F}}{\partial x} + \frac{\partial \mathbf{G}}{\partial y} = \mathbf{S} \tag{1}$$

$$\mathbf{U} = \begin{bmatrix} h \\ h\bar{v}_x \\ h\bar{v}_y \end{bmatrix} \qquad \mathbf{F} = \begin{bmatrix} h\bar{v}_x \\ h\bar{v}_x^2 + \frac{1}{2}hc^2 \\ h\bar{v}_x\bar{v}_y \end{bmatrix} \qquad \mathbf{G} = \begin{bmatrix} h\bar{v}_y \\ h\bar{v}_y\bar{v}_x \\ h\bar{v}_y^2 + \frac{1}{2}hc^2 \end{bmatrix} \qquad \mathbf{S} = \begin{bmatrix} 0 \\ S_x \\ S_y \end{bmatrix} \tag{2}$$

where

$$\begin{aligned} S_x = {} & g_x h - \mathrm{sgn}(\bar{v}_x)(1-\lambda)\left(g_z + \bar{v}_x^2 \frac{\partial \theta_x}{\partial x}\right) h \tan\varphi_{bed} - \frac{3\upsilon_f \mu}{\rho}\frac{\bar{v}_x}{h} \\ & + \frac{\upsilon_f \mu h}{\rho}\frac{\partial^2 \bar{v}_x}{\partial x^2} + \mathrm{sgn}\left(\frac{\partial^2 \bar{v}_x}{\partial y^2}\right) h k_{act/pass} \frac{\partial}{\partial y}[g_z h(1-\lambda)]\sin\varphi_{int} + \frac{\upsilon_f \mu h}{\rho}\frac{\partial^2 \bar{v}_x}{\partial y^2} \end{aligned} \tag{3}$$

$$\begin{aligned} S_y = {} & g_y h - \mathrm{sgn}(\bar{v}_y)(1-\lambda)\left(g_z + \bar{v}_y^2 \frac{\partial \theta_y}{\partial y}\right) h \tan\varphi_{bed} - \frac{3\upsilon_f \mu}{\rho}\frac{\bar{v}_y}{h} \\ & + \frac{\upsilon_f \mu h}{\rho}\frac{\partial^2 \bar{v}_y}{\partial y^2} + \mathrm{sgn}\left(\frac{\partial^2 \bar{v}_y}{\partial x^2}\right) h k_{act/pass} \frac{\partial}{\partial x}[g_z h(1-\lambda)]\sin\varphi_{int} + \frac{\upsilon_f \mu h}{\rho}\frac{\partial^2 \bar{v}_y}{\partial x^2} \end{aligned} \tag{4}$$

$$\lambda = \frac{p_{bed}}{\rho g_z h} \tag{5}$$

$$k_{act/pass} = 2\frac{1 \mp [1 - \cos^2\varphi_{int}(1 + \tan^2\varphi_{bed})]^{1/2}}{\cos^2\varphi_{int}} - 1 \tag{6}$$

$$c = \sqrt{[(1-\lambda)k_{act/pass} + \lambda]g_z h} \tag{7}$$

In these equations the independent variables are time t and the space coordinates x and y. The dependent variables are the depth-averaged velocity components $\bar{v}_x(x,y,t)$ and $\bar{v}_y(x,y,t)$ and the flow depth $h(x,y,t)$ in the z direction, normal to the bed (Figure 1). The function sgn used in (3) and (4) designates the sign (+ or -) of its argument.

The basic parameters in the governing equations are the components of gravitational acceleration, g_x, g_y, and g_z; the components of the local bed slope, θ_x and θ_y (measured in radians from the horizontal); the internal and basal friction angles of the solid grains, φ_{int} and φ_{bed}; the viscosity and volume fraction of the intergranular fluid, μ and υ_f; and the bulk density of the grain-fluid mixture, ρ. These fundamental, measurable parameters are used to derive the other coefficients in (1)-(4), which are defined in (5)-(7). The coefficient λ represents the ratio of the basal pore-fluid pressure, p_{bed}, to the total basal normal stress, $\rho g_z h$. Values of λ vary as a function of x, y, and t and are obtained by computing p_{bed} using an advection-diffusion equation described below. The longitudinal stress coefficient $k_{act/pass}$ is derived from Coulomb failure theory and determines the magnitude of grain-contact normal stresses in the x-y plane (Iverson, 1997). Typically, values of $k_{act/pass}$ exceed 1 where flow locally converges ($k = k_{pass}$) but are less than 1 where flow locally diverges ($k = k_{act}$). As a result, depth-averaged longitudinal stresses in grain-fluid mixtures are more complicated than those in one-phase fluid flows. The coefficient c is the gravity-wave speed that determines the rate of longitudinal information propagation in the flow. The equation defining c is more complicated than the analogous equation for fluid flows, owing to the effects of longitudinal grain stresses and variable fluid pressure. However, the definition of c reduces to the standard shallow-water definition $c = \sqrt{g_z h}$ if the grain-fluid mixture is fully liquefied ($\lambda = 1$) and Coulomb grain-contact stresses vanish.

The most obvious difference between (1)-(4) and the conventional shallow-water equations exists in the source terms, S_x and S_y, which represent the sum of driving and resisting forces per unit area of the bed (divided by ρ). The equations defining S_x and S_y each contain six terms. In order, these terms have the following physical significance: 1. gravitational driving force; 2. resisting force due to granular Coulomb friction at the bed, which is influenced by bed curvature; 3. resisting force due to viscous fluid drag resolved at the bed; 4. longitudinal normal force due to viscous fluid elongation or compression in the direction of flow; 5. intergranular Coulomb force due to velocity gradients transverse to the direction of flow; and 6. viscous fluid force due to velocity gradients transverse to the direction of flow. Forces associated with longitudinal stress gradients due to variations in h are excluded from S_x and S_y and instead are contained within c, as noted above.

In S_x and S_y the terms involving space derivatives of bed slope account for all effects of bed curvature (e.g., $\partial\theta_x/\partial x = 1/r_x$, where r_x is the x component of the local radius of curvature; Figure 1). These curvature terms represent the effects of coordinate transformations that show how changes in bed slope redirect x and y momentum components to keep them parallel to the bed (e.g., Savage and Hutter, 1991). Redirection of the x and y momentum components influences basal normal stresses and thereby produces changes in Coulomb resistance and flow thickness. Where finite changes in bed slope occur between adjacent computational cells, we use the approximation $\partial\theta_x/\partial x \approx \tan(\Delta\theta_x/\Delta x)$ to account for curvature of the bed (Denlinger and Iverson, 2000).

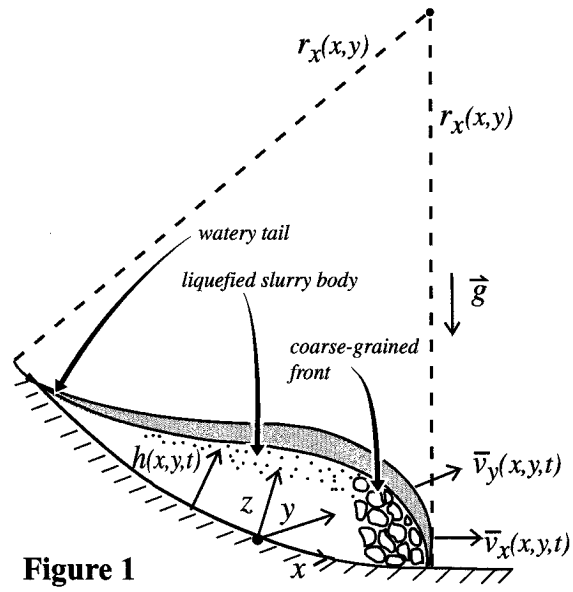

Figure 1

Evaluation of λ: The basal fluid-pressure ratio $\lambda = p_{bed}/\rho g_z h$ defined in (5) must be evaluated simultaneously with the dependent variables that describe flow, $\bar{v}_x(x,y,t)$, $\bar{v}_y(x,y,t)$ and $h(x,y,t)$. Guided by observations and measurements in large-scale experiments (Iverson, 1997; Major and Iverson, 1999), we infer that basal fluid pressures advect with depth-averaged flow and simultaneously diffuse normal to the bed, obeying (Iverson and Denlinger, 2000)

$$\frac{\partial p_{bed}}{\partial t} + \bar{v}_x \frac{\partial p_{bed}}{\partial x} + \bar{v}_y \frac{\partial p_{bed}}{\partial y} = D \frac{\partial^2 p}{\partial z^2}\Big|_{bed} \tag{8}$$

where $|_{bed}$ designates that the diffusion term is evaluated at the bed, where $z = 0$. The pore-pressure diffusivity, D, determines the rate of pressure diffusion and is defined by $D = kE/\mu$, where k is the intrinsic hydraulic permeability of the aggregate solid debris and E is its compressive stiffness. For typical debris-flow mixtures D has values in the range 10^{-7}-10^{-3} m^2/s (Iverson, 1997; Major et al., 1997). These values imply, for example, that excess fluid pressures in flows 1 m thick can persist for times ranging from minutes to months, once excess pressures are established. (Excess fluid pressures are those in excess the hydrostatic fluid pressure, $p_{bed} = \rho_{fluid} g_z h$. This hydrostatic pressure is less than the total basal pressure $\rho g_z h$ used to define λ, because the fluid density ρ_{fluid} is less than the total mixture density, ρ.) Excess fluid pressures are generally established during the initial stages of debris-flow motion due to soil contraction and liquefaction (Iverson et al., 2000).

Modification for Flash Floods: Fluid forces play a different role in flash floods than in debris flows because volumetric sediment concentrations in the body of flash floods are too low to form an interconnected granular matrix. Therefore, in the body of flash floods, Coulomb grain-contact forces are negligible and pore-pressure diffusivity is irrelevant. Consequently, we infer that fluid pressures are uniformly hydrostatic (the usual shallow-water assumption) in the body of flash floods and that suspended solids merely increase the fluid density. We also infer that turbulent energy dissipation is important in flash floods, and that the viscous resistance terms in (3) and (4) must be replaced by

terms representing the effects of turbulence. Adopting turbulence terms suggested by Vreugdenhil (1994), we reduce (3)-(7) to forms applicable to the watery body of flash floods

$$S_x = g_x h - s_f \bar{v}_x \sqrt{\bar{v}_x^2 + \bar{v}_y^2} \tag{9}$$

$$S_y = g_y h - s_f \bar{v}_y \sqrt{\bar{v}_y^2 + \bar{v}_x^2} \tag{10}$$

$$\lambda = 1 \tag{11}$$

$$k_{act/pass} = 1 \tag{12}$$

$$c = \sqrt{g_z h} \tag{13}$$

These relationships demonstrate that the standard shallow-water equations are a special case of our debris-flow equations (modified to account for fluid turbulence).

The dimensionless turbulent stress coefficient s_f used in (9) and (10) depends on relative boundary roughness and Reynolds number, and its value cannot, in general, be specified without some estimate of flow speeds and depths. However, for flows on rough beds at high Reynolds numbers ($> 10^5$), values of s_f commonly are of the order of 0.1. For flows across rugged terrain, exact values of s_f are relatively unimportant because multidimensional momentum transport described by equations (1) and (2) accounts for the effect of topography on water-surface slopes (Denlinger et al., 1998).

If the leading margin of a flash flood scours or abrades stream banks or the bed and thereby acquires substantial quantities of woody debris or coarse sediment, the flood wave may act somewhat like a debris flow with a high-friction snout and low-resistance tail. To model the mechanics of a debris-laden bore, equations (9)-(13) can be blended with the more general equations (3)-(7). In this case values of the basal fluid-pressure ratio vary from $\lambda = 0$ at the leading edge of the bore, where solid Coulomb friction dominates resistance, to $\lambda = 1$ in the part of the flood where fluid turbulence dominates resistance. For flash floods, of course, energy dissipation due to fluid forces is modeled using the turbulent stress terms in (9) and (10) rather than the viscous stress terms in (3) and (4).

Discrimination of Bore Fronts: A key step in computing motion of debris flows and flash floods with debris-laden bores involves discrimination of bore-front regions with low values of λ and high Coulomb friction. Equation (8) with constant pore-pressure diffusivity is insufficient for this purpose. According to (8), the only factors affecting the distribution of λ are initial conditions, downstream pressure advection, and the local flow thickness and pore-pressure diffusivity. To these factors we add kinematic criteria for identifying fronts of bores, which we infer have elevated diffusivities and depleted pore pressures. We identify fronts of bores as those regions where flow thickness decreases in the downstream direction. Such regions satisfy one or more of the kinematic criteria

$$\begin{aligned} \bar{v}_x > 0 \quad &\text{and} \quad \partial h/\partial x < 0 \\ \bar{v}_x < 0 \quad &\text{and} \quad \partial h/\partial x > 0 \\ \bar{v}_y > 0 \quad &\text{and} \quad \partial h/\partial y < 0 \\ \bar{v}_y < 0 \quad &\text{and} \quad \partial h/\partial y > 0 \end{aligned} \tag{14}$$

Where such criteria are met, we increase D significantly (typically by 1-2 orders of magnitude) before solving (8). In the extreme case of a bore composed entirely of large rocks or woody debris, we assume that D is essentially infinite and that no fluid pressure can be sustained. This simplistic assumption yields relatively good predictions of debris-flow motion (Denlinger and Iverson, 2000).

Mass Change (Erosion and Sedimentation): Debris flows and debris-laden flash floods can significantly change their mass by entraining or depositing debris in transit, and mass change may significantly affect flow dynamics. Mass change is a three-dimensional process. Field observations indicate that flow mass typically increases as a result of undermining and scouring channel banks, and that flow mass decreases progressively where channels widen or slopes decline.

Mass-change terms can be added with little difficulty to the momentum and mass balances expressed in (1) and (2), but a significant difficulty attends use of such terms. Mass change depends on poorly constrained external forces that govern substrate strength and influence momentum transfer between the flowing mass and its three-dimensional boundaries (Iverson, 1997). These external forces must be included in models that compute adjustments of the basal boundary position due to erosion and sedimentation. For the present, we ignore the possibility of mass change and focus on the simpler case in which boundaries are fixed and flow mass is constant. Evaluation of forces associated with mass change remains an outstanding problem that must be solved to develop a complete understanding of the dynamics of debris flows and flash floods.

NUMERICAL SOLUTION TECHNIQUE

The nonlinear, hyperbolic partial differential equations (1)-(4) require special techniques for numerical solution in arbitrarily complex domains such as those imposed by three-dimensional flow-path topography. We use a technique that constructs solutions throughout complex flow domains by solving elementary Riemann problems that govern the magnitudes and directions of mass and momentum fluxes through the walls of individual computational cells (Toro, 1997). Elsewhere, we describe details of our technique (Denlinger and Iverson, 2000). Here we outline some aspects of the technique that are particularly important for computing motion of debris flows and flash floods.

The Riemann methodology recasts equations (1) and (2) in terms of Jacobian matrices **A** and **B**. Then (1) becomes

$$\frac{\partial \mathbf{U}}{\partial t} + \mathbf{A} \cdot \frac{\partial \mathbf{U}}{\partial x} + \mathbf{B} \cdot \frac{\partial \mathbf{U}}{\partial y} = \mathbf{S} \tag{15}$$

where

$$\mathbf{A} = \begin{bmatrix} 0 & 1 & 0 \\ c^2 - \bar{v}_x^2 & 2\bar{v}_x & 0 \\ -\bar{v}_x\bar{v}_y & \bar{v}_y & \bar{v}_x \end{bmatrix} \qquad \mathbf{B} = \begin{bmatrix} 0 & 0 & 1 \\ -\bar{v}_x\bar{v}_y & \bar{v}_y & \bar{v}_x \\ c^2 - \bar{v}_y^2 & 0 & 2\bar{v}_y \end{bmatrix} \tag{16}$$

The Riemann problem consists of first computing the trajectories along which information about the conserved variables **U** propagates in space and time (given by eigenvectors of **A** and **B**), and then balancing fluxes of the conserved variables along these trajectories. Explicit Euler integration incorporates the effects of the source terms, **S**, and advances the solution in time. This approach has great advantages for minimizing numerical dispersion and tracking shocks. Accurate shock tracking is more important for predicting behavior of debris flows and flash floods than is typically the case for slower water floods. Prevalence of steep flow paths, abrupt flow fronts, severe topographic obstructions, and variability of the gravity-wave speed, c, commonly causes shock-rich behavior in debris flows and flash floods.

Numerous techniques have been devised for numerical solution of Riemann problems (Toro 1997). Techniques differ chiefly according to the scheme used to balance fluxes across grid-cell boundaries. We use a technique (called HLLC) that generates approximate solutions to exact Riemann problems involving the nonlinear terms in **A** and **B** (Toro, 1997). Denlinger and Iverson (2000) provide details of our implementation of the HLLC solver.

Flow-front Propagation Speeds: Debris flows and flash floods have sharply defined flow fronts, which pose unique challenges for predictive models. Numerically, such fronts occur wherever zero flow depth exists adjacent to a computational cell. Our means of computing the speeds of these fronts follows a rationale like that of Toro (1997, p. 140) for an analogous problem involving vacuum fronts in shock tubes. Here we focus on the equation governing the speed of a flow front advancing in the right-hand (positive x) direction, but analogous equations apply to advancing and receding fronts in all directions.

Mass and momentum conservation dictate that physical information emanating from flow fronts propagates in a manner that preserves a quantity (known as a Riemann invariant) defined by

$$I_L = \bar{v}_x|_L + 2c_L \tag{17}$$

for the case $S_x = 0$. Here the subscript L denotes waves moving left (upstream) from the flow front. Very near the flow front (where $h \to 0$ and $\upsilon_f \to 0$), it is reasonable to assume that $S_x \to 0$, and we therefore assume that I_L is approximated well by (17). We then equate values of I_L at the flow front (denoted by subscript 0) and at any other point just upstream of the flow front, yielding

$$\bar{v}_x|_0 + 2c_0 = \bar{v}_x|_L + 2c_L \tag{18}$$

However, near the flow front the gravity wave speed c approaches zero because $h \to 0$, and precisely at the front, $c_0 = 0$ exactly. Substituting this value in (18) and combining the result with (17) yields

$$\bar{v}_x|_0 = I_L \tag{19}$$

which indicates that the speed of the mixture at the flow front equals the Riemann invariant associated with the left-going waves emanating from the flow front. Moreover, since the mixture thickness tapers to zero at the flow front, the mixture speed equals the speed of the front itself. Effectively, the speed of the right-going front is dictated by the rate at which material discharges from the left.

CONCLUDING DISCUSSION

This paper highlights key features of a mathematical model we have developed to simulate motion of debris flows and debris-laden flash floods. Elsewhere, we describe details of model formulation and tests of model predictions against experimental data for dry granular avalanches and water-saturated debris flows (Iverson and Denlinger, 2000; Denlinger and Iverson, 2000). Here we introduce model modifications necessary to simulate motion of debris-laden flash floods. In all cases a central feature of the model is use of depth-averaged mass- and momentum-conservation equations applicable to flow over three-dimensional terrain. Another key feature is use of a Riemann solution algorithm that does not restrict model applications to smooth or gently sloping beds. These features appear crucial for extending the model to analyze flows that change mass as they move through realistic landscapes.

REFERENCES

Denlinger, R.P., Walters, R.A., Ostenaa, D., Levish, D., 1998, Robust methods for routing floods over highly irregular terrain, *Proceedings of the First Federal Interagency Conference on Floods*, Las Vegas, Nevada, April, 1998. 6-89 - 6-95.

Denlinger, R.P., Iverson, R.M., 2000, Flow of variably fluidized granular masses across 3-D terrain: 2. Model predictions and experimental tests, *Journal of Geophysical Research (B)*, in press.

Iverson, R.M., 1997, The physics of debris flows, *Reviews of Geophysics*, 35, 245-296.

Iverson, R.M., Denlinger, R.P., 2000, Flow of variably fluidized granular masses across 3-D terrain: 1. Coulomb mixture theory, *Journal of Geophysical Research (B)*, in press

Iverson, R.M., Reid, M.E., Iverson, N.R., LaHusen, R.G., Logan, M., Mann, J.E., Brien, D.L., 2000, Acute sensitivity of landslide rates to initial soil porosity, *Science*, in press.

Major, J.J., Iverson, R.M., 1999, Debris-flow deposition: effects of pore-fluid pressure and friction concentrated at flow margins, *Geological Society of America Bulletin*, 111, 1424-1434.

Major, J.J., Iverson, R.M., McTigue, D.F., Macias, S., and Fiedorowicz, B.K., 1997, Geotechnical properties of debris-flow sediments and slurries, *in Debris-flow Hazards Mitigation: Mechanics, Prediction, and Assessment*, C.L. Chen, ed., American Society of Civil Engineers, 249-259.

Savage, S.B., Hutter, K., 1991, The dynamics of avalanches of granular materials from initiation to runout, Part I. analysis, *Acta Mechanica,* 86, 201-223.

Toro, E.F., 1997, *Riemann Solvers and Numerical Methods for Fluid Dynamics*, Springer-Verlag, 492 p.

Vreugdenhil, C.B., 1994, *Numerical Methods for Shallow-water Flow*, Kluwer, 261 p.

THE RAINFALL-TRIGGERED LANDSLIDE AND FLASH FLOOD DISASTER IN NORTHERN VENEZUELA, DECEMBER 1999

By M.C. Larsen, Hydrologist, (1) G.F. Wieczorek, Engineering Geologist, (2) L.S. Eaton, Geologist, (3) H. Torres-Sierra, Hydrologist, (1)
(1) U.S. Geological Survey, Guaynabo, Puerto Rico, USA, (2) U.S. Geological Survey, Reston, Virginia, USA, (3) James Madison University, Harrisonburg, Virginia, USA, mclarsen@usgs.gov, fax: 787-749-4301

Abstract: Rainstorms in December 1999 induced thousands of landslides along the northern slopes of the Cordillera de la Costa mountain range principally in the state of Vargas, Venezuela. Rainfall accumulation of 293 millimeters during the first 2 weeks of December was followed by an additional 911 millimeters of rainfall on December 14 through 16. The landslides and floods inundated coastal communities resulting in a catastrophic death toll estimated at between 15,000 and 30,000 people. Debris flow damage to houses, buildings, and infrastructure in the narrow coastal zone was severe. Flash floods on alluvial fans at the mouths of rivers draining the coastal mountain range also contributed to the general destruction.

In time scales spanning decades to centuries, the alluvial fans along this Caribbean coastline are areas of high geomorphic activity. Because most of the coastal zone in Vargas consists of steep mountain fronts that rise directly from the Caribbean Sea, the alluvial fans provide the only relatively flat areas upon which to build. Rebuilding and reoccupation of these areas requires careful determination of hazard zones to avoid future loss of life and property. A limited assessment of the distribution and character of landslides is currently in progress by the U.S. Geological Survey in cooperation with the Venezuelan Ministry of Environment and Natural Resources.

INTRODUCTION

Several hundred thousand people reside in a narrow coastal zone north of Caracas, Venezuela, in the state of Vargas. Located at the base of steep mountains, the population is highly vulnerable to episodic rainfall-induced landsliding. In December 1999, the interaction of a cold front with moist southwesterly flow from the Pacific Ocean towards the Caribbean Sea resulted in an usually wet period over northern Venezuela. Rainfall accumulation at sea level on the Caribbean coast at the Maiquetía airport for the first 2 weeks of December was 293 mm, more than five times the average (MARN, 2000). An additional 911 mm of rainfall was recorded from December 14-16. On December 15-16, 1999, landslides (mostly debris flows) and flash floods along the northern coastal zone of the Cordillera de la Costa in the state of Vargas and neighboring states in northern Venezuela (fig. 1) killed thousands of people, caused extensive property damage, and changed hillslope, stream channel and alluvial fan morphology. Because no census data are available for many of the affected areas, and because many of the dead were either buried under meters of rocky debris or washed out to sea, the death toll will never be known precisely. Current estimates indicate that as many as 30,000 lives were lost (USAID, 2000).

LANDSLIDE CHARACTERISTICS

Landslides caused by the rainstorm numbered in the thousands in the Cordillera de la Costa, which parallels the north coast. The landslides were mainly debris flows of a few meters or less in depth but 100's of meters in length, and shallow soil slips, which were generally a few meters or less in thickness but, in many cases, 100's of meters in width. The majority of debris flows began as either shallow debris slides or soil slides (slips). As such, many landslides affected the entire length of the hillslope from crest to toe. Hillslopes measured in a sample of 26 landslides had a mean slope angle of 42º (standard deviation of 7.6º). Coalescing debris flows moved rapidly down steep narrow canyons with step-pool morphology. The canyon floor gradients average 5º to 10º in reaches 3 to 6 kilometers upstream of their alluvial fans. Further upstream, steep waterfalls in bedrock prevented additional reconnaissance. In the last several km south of their alluvial fans, channel slopes average 4º to 6º and decrease to 2º to 4º across the fans before reaching the Caribbean Sea.

Most of the landslide scars are on the north side of the mountain range including large areas in El Avila National Park. Although several small communities, San José de Galipán and San Francisco de Galipán, are located within the Park boundary, most of the Park is undeveloped forest. As such, deaths attributed directly to landslides in steeply sloping areas comprised only a small fraction of the total loss of life estimated in the disaster. Landslides also destroyed or damaged many kilometers of the two-lane highway that links coastal communities east of Maiquetía.

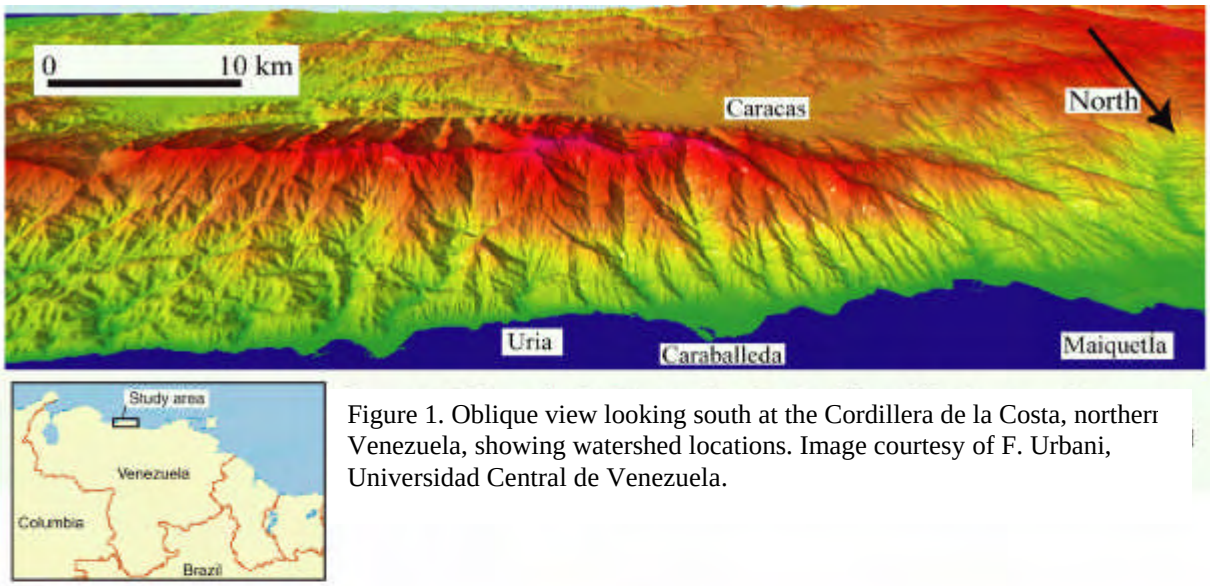

Figure 1. Oblique view looking south at the Cordillera de la Costa, northern Venezuela, showing watershed locations. Image courtesy of F. Urbani, Universidad Central de Venezuela.

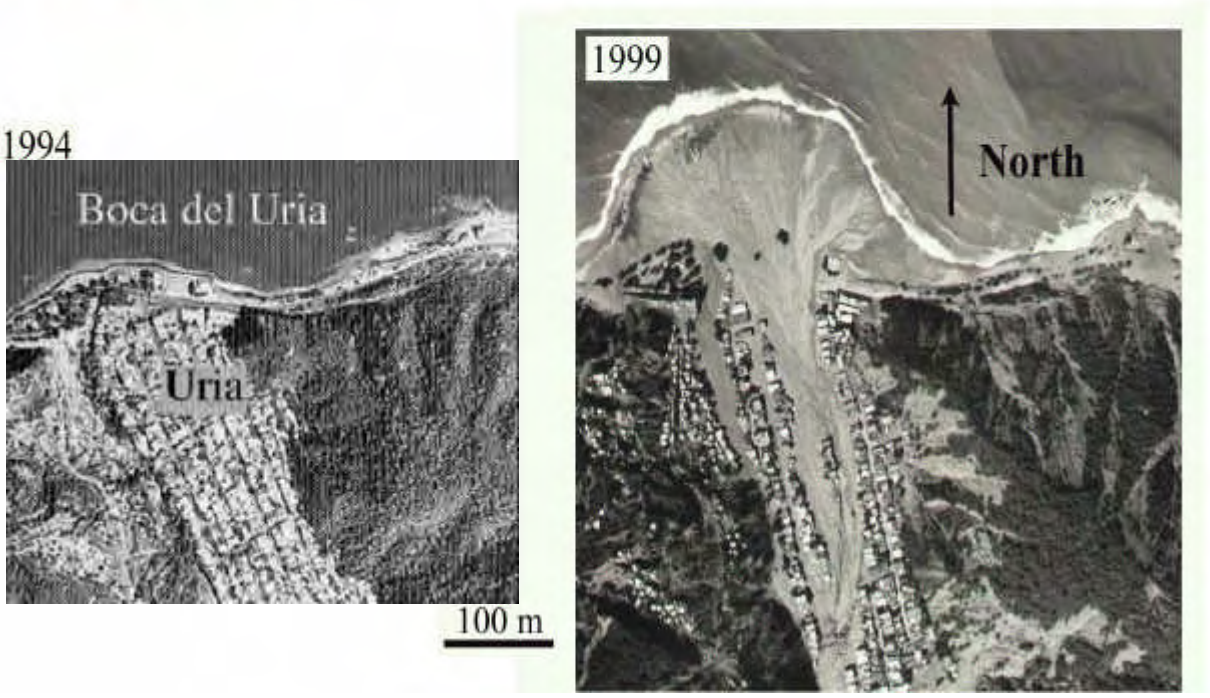

Figure 2. Aerial photographs taken in 1994 and after the December 1999 event showing destruction of the Carmen de Uria community and shoreline progradation (MARN-SAGECAN, 2000). Photograph (1999) courtesy of F. Urbani, Universidad Central de Venezuela (1999).

Rescue and initial relief efforts were severely hampered because of the lack of ground access. Much of the road was opened to traffic by March 2000; however, along the road corridor east of Naiguata, landslide damage to the highway was extreme and rehabilitation will require extensive reconstruction.

FLASH FLOODS

Flash floods and debris flows occurred in most of the several dozen small catchments (watershed areas on the order of 10 to 30 km^2) that drain the Cordillera de la Costa mountain range north to the Caribbean Sea. The stream-channel gradients in these catchments range from 20 to 50 percent (11 to 27 degrees); headwater elevations range from 2,000 to 2,700 meters and drop to sea level across a distance of 6 to 12 km (MARN, 2000). After passing through narrow canyons, streams emerging at the mountain front only a few tens of meters above sea level drain onto low-gradient (2 to 4 degrees) alluvial fans. High water marks left by flash floods were noted in the downstream canyons of 10 watersheds. Peak flow depths were as great as 8 to 10 m in canyon reaches that were on the order of 50 m wide. Channel slopes in these reaches were between 4 and 6 degrees. Residents with homes at the mouths of the 10 watersheds generally reported episodic high stream flows that began late on the night of December 15 and continued until the afternoon of December 16. Although each of the watersheds showed evidence of massive debris flows, most also contained laminar, well stratified flood deposits, indicating that both flood and debris flow processes were common.

VULNERABILITY OF POPULATION AND INFRASTRUCTURE

Because most of the coastal zone in the Vargas state consists of steep mountain fronts that rise directly from the Caribbean Sea, the alluvial fans provide the only flat areas upon which to build. A major airport at Maiquetía and seaport facilities have been constructed on these fans and a few available stretches of narrow coastal plain. In addition, housing that ranges from unregulated shanty towns, to middle- and upper-income single-family dwellings, to multi-story apartment buildings and condominiums, to hotels has been concentrated in communities along the coast east of Maiquetía (fig. 1). These residential and vacation communities are where most of the damage and loss of life occurred (figs. 2,3,4).

A combination of debris flows that transported massive boulders, and flash floods carrying extremely high sediment loads were the principal agents of destruction. On virtually every alluvial fan along 50 km of coastline, rivers incised new channels into fan surfaces to depths of several meters, and massive amounts of new sediment were disgorged upon fan surfaces in quantities of up to 15 metric tonnes per square meter (fig. 5). Sediment size ranged from clay and sand to boulders as large as 10 meters in diameter (figs. 5,6). Hundreds of houses, bridges and other structures were damaged or obliterated. Because residents had little warning in advance of the debris flows and flash floods that struck during in the early hours of December 16, many were caught in their homes and their bodies were carried out to sea or buried in the flood debris.

Carmen de Uria and Caraballeda are two of the many communities impacted by debris flows and flash floods. These two well-known areas provide insight into the types of damage that the coastal region incurred.

Carmen de Uria

Carmen de Uria is a small community dominated by lower-income housing built on a narrow alluvial fan between steep canyon walls at the mouth of an 11.9 km^2 watershed (fig. 2). Dozens of homes in a section of the central fan were obliterated by debris flows that survivors said occurred in two to three episodes between midnight and 9 am on December 16 (fig. 3). Before that date, the large open area, visible in figures 2 and 3 had a housing density comparable to that seen in the southeast section of figure 2.

The mass of debris flow and flood-transported sediment built the shoreline seaward by as much as 100 m and deposited a new subaerial delta of approximately 233,000 m^3, assuming a 20 degree submarine slope. This volume of deposition indicates a minimum erosion depth of 20 mm averaged over the entire watershed. The actual number is likely to be substantially higher as the submarine section of the delta distal to the new shoreline was not included, nor were the portions of the sediment load that were transported offshore.

Figure 3. Aerial and ground views showing debris flow and flash flood damage at Carmen de Uria, January 2000.

Figure 4. Aerial image taken after December 1999 event showing the Caraballeda fan and destruction of the Los Corales community. Image courtesy of F. Urbani, Universidad Central de Venezuela.

Figure 5. Debris flow deposits on the Caraballeda fan. (A) House with 1-m diameter boulders on roof. (B) Concrete house rotated off foundation by debris flow. (C) View across debris fan; tiled surface on right is top of one story home. (D) View up debris fan looking towards San Julián Canyon.

Caraballeda

On the Caraballeda alluvial fan, 10 km west of Carmen de Uria, extensive property destruction occurred (figs. 4,5). Approximately 1.25 million m^3 of debris flow deposits, which included numerous massive boulders up to 10 m long, were distributed across several square kilometers of fan surface resulting in a deposit thickness of up to 4 m (fig. 5). Small structures were reduced to rubble in many cases and large, multi-story apartment buildings sustained heavy damage (fig. 6). The thickness of debris flow deposits measured at locations within 150 m of the current shoreline averaged 1.5 to 2 m, and the diameter of the largest boulders (D_{90}) at sites near the shoreline was on the order of 1 m. An estimated 450,000 m^3 of sediment was deposited in a 1,000-m wide subaerial delta with an average seaward extent of 50 m, assuming the same 20 degree submarine slope used for the estimate at Carmen de Uria.

PREVIOUS DEBRIS FLOW EVENTS

Exposures of old debris flow deposits were ubiquitous along canyon walls and on dissected alluvial fan surfaces (figs. 7,8). These deposits are strong physical evidence for the episodic recurrence of debris flow events in the Cordillera de la Costa. Deposits from a high-magnitude prehistoric debris flow event were observed in a number of watersheds (fig. 8). The deposits included massive boulders, larger than those moved in the December 1999 event, and indicate that although the 1999 event was rare, a more extreme storm event occurred in prehistoric time.

Over time scales spanning decades to centuries, the alluvial fans are dynamic zones of high geomorphic activity (Audemard and others, 1988; Singer and others, 1983). On average, at least one or two high-magnitude flash-flood

and landslide events per century have been recorded in this region since the 17th century. In the nearby states of Aragua and Carabobo, destructive flash flood and landslide events were recorded in 1693, 1789, 1798, 1804, 1808, 1812, 1890, 1892, 1902, 1912, 1914, 1927, 1933, 1945, 1946, 1951, 1956, 1962 and 1963 (Röhl, 1950; Garner, 1959; Audemard and others, 1988). Another 13 high-magnitude events were recorded during the 1970's.

Using Spanish archives, Röhl (1950) provided a detailed summary of flash floods and debris flows that caused extensive damage to homes and government buildings and destroyed all bridges in La Guaira in 1798. A series of floods and debris flows occurred over a 2-day period. and were so large that Spanish soldiers placed cannons cross-wise in front of the upstream-facing entrance to a fort constructed near the stream channel to barricade the structure.

Northern Venezuela lies within a region where an average of 50 thunderstorms per year are documented for any point on the land surface (Hayden, 1988). In this region, high-intensity rainfall events with decadal-scale return frequencies erode upstream hillslopes and transport massive amounts of sediment onto aggrading and prograding alluvial fans. In this dynamic environment, population and infrastructure are highly vulnerable by these episodic large-magnitude storms such as that which occurred in December.

SUMMARY

A combination of climatologic, geologic, and demographic factors makes the Caribbean coast of Venezuela in the state of Vargas highly susceptible to episodic debris flows and flash floods. An extremely steep, tectonically active mountain front forms the boundary with a tropical sea. Easterly tradewinds can force moist air masses upslope and precipitate large rainfall volumes, creating conditions for high-magnitude debris flows and flash floods. The population of several hundred thousand people that reside at the base of the mountains is inevitably vulnerable to hydrologic disasters that seem to recur once or twice per century. The flash flood-debris flow process combination is highly destructive in populated areas. Without careful planning of human settlements, the impacts of these types of disasters are likely to increase in the future.

ACKNOWLEDGEMENTS

This work was supported by the USGS, the Venezuela Ministry of Natural Environment, and the USAID Office of Foreign Disaster Assistance. Special thanks are expressed to Prof. Franco Urbani, Universidad Central de Venezuela, for his enthusiam in the field, geologic insights, and for the extensive data he provided to the authors. Helpful review comments were provided by Joseph W. Troester and Benjamin A. Morgan, USGS. Gratitude is expressed to Colonel Romer Mena Nava and Dr. Alicia Moreau, Servicio Autónomo de Geografía y Cartografía Nacional, Ministerio del Ambiente y de los Recursos Naturales,Venezuela, for facilitating the helicopter overflights in coastal Venezuela, January 2000 and numerous field trips between January and August 2000.

REFERENCES

Audemard, F.A., De Santis, F., Montes, L., Lugo, M. and Singer, A., 1988, El Alud Torrencial del 6-9-1987 del Río Limón, al norte de Maracay, Estado Aragua. *Informe Interno FUNVISIS* (Fundación Venezolana de Investigaciones Sísmicas), 9 p.

Garner, H.F., 1959, Stratigraphic-Sedimentary Significance of Contemporary Climate and Relief in Four Regions of the Andes Mountains. Geological Society of America Bulletin, 70, 10, 1327-1368.

Hayden, B.P., 1988, Flood Climates, In Baker, V.R., Kochel, R.C., and Patton, P.C., (Eds.), Flood Geomorphology. John Wiley and Sons, New York, 13-26.

MARN, 2000, Informe Preliminar Sobre los Aspectos Ambientales Vinculadas al Desastre Natural Ocurrido en Venezuela Durante el Mes de Diciembre de 1999. Ministerio del Ambiente y de los Recursos Naturales, Venezuela, unpublished report, 55 p.

MARN-SAGECAN, 2000, Crónica Crtográfica de la Catástrofe de Venezuela. Ministerio del Ambiente y de los Recursos Naturales, Servicio Autónomo de Geografía y Cartografía Nacional, Venezuela, 15 p.

Röhl, E., 1950, Los Diluvios en las Montañas de la Cordillera de la Costa. Boletín de la Academia de Ciencias Físicas, Matemáticas y Naturales, Venezuela, 38, 1-28.

Singer, A, Rojas, C., and Lugo, M., 1983, Inventario Nacional de Riesgos Geológicos, Mapa, Glosario y Comentarios. Serie Técnica FUNVISIS, (Fundación Venezolana de Investigaciones Sísmicas)03-83, Caracas, Venezuela, 126 p.

USAID, 2000, Venezuela Factsheet, February, 2000. USAID-Office of Foreign Disaster Assistance, 2 p.

Figure 6. Apartment building damaged by debris flows Caraballeda. Note collapsed apartments and boulders on floor of second story.

Figure 7. House and garage on Caraballeda fan with exposed foundation showing old debris flow deposit.

Figure 8. Massive boulders deposited by ancient debris flow in the RÍo San Julian valley, approximately 2 k upstream of Caraballeda. The boulders were exposed by the December 1999 event. Their dimensions exceed that of the largest boulders moved in December 1999. Note person on left for scale.

LARGE RIVERS AND THEIR FLOODPLAINS AS CONVEYERS AND STORERS OF SEDIMENT: AN OVERVIEW

ROBERT H. MEADE
US Geological Survey
MS 413, Box 25046, Federal Center
Denver, Colorado 80225-0046
USA

Abstract. Large rivers are continental-scale conveyance systems for moving sediment. Sources of sediment in these systems are heterogeneous and variable in space and time. Between original source and ultimate sink, river sediment can be subjected to multiple episodes of storage into and remobilization out of floodplains and other alluvial features. Exchanges of sediment between channels and floodplains, in sufficiently long reaches of river, can store and remobilize quantities of sediment that are greater than the net downriver fluxes. Residence times of sediment in storage may be sufficiently long (i.e., millennia) in some floodplains to allow the pedochemical transformation of mineral compositions of sediment particles. In the lowest reaches of most large river systems, floodplains are net sinks for riverine sediment. The seaward transfers of river sediment into deltas, estuaries, and onto continental shelves are complex responses to oceanic tides, coastal currents, and the spatial configurations of coastlines.

INTRODUCTION

Large rivers are massive conveyance systems for moving sediment across transcontinental distances. In South America, for example, the three largest river systems (Orinoco, Amazon, Paraguay-Paraná) transfer sediment from the leading edge (active margin) to the trailing edge (passive margin) of a drifting continent (Potter, 1978, 1998). Matching the large spatial scales are the temporal scales of alluvial storage, on the order of 10^3 -10^4 years, that retard the conveyance of sediment from original source to ultimate sink.

Knowledge of sediment in large rivers is pertinent to many practical issues. In earlier decades, the compelling reasons for studying sediment were almost exclusively related to devebpmental uses such as hydropower, navigation, crop irrigation, and soil erosion. In more recent years in the more developed regions of the world, two of the largest societal issues around which sediment research is becoming focused are (1) the role of sediment in the transport and sequestering of adsorbed contaminants, and (2) the role of sedimentary processes in the construction, preservation, and destruction of habitats. The fundamental questions, however, remain unchanged: How much sediment passes down the river system, and where does it come from? How is it transported? How long does it spend in transit or in a variety of storage sites? How and where does it finally come to rest? In the following discussion, the lack of graphic illustration will be compensated by intensive bibliographic references to pertinent figures published elsewhere.

SOURCES OF SEDIMENT

Sources of water and sediment in most of the great river systems of the world are distributed unevenly in space. The Mississippi River basin, for example, lies athwart such a large rainfall gradient that some of the western tributaries receive only a fourth to a third the rainfall received by some of the eastern tributaries. The Missouri River basin contributes only 15% of the total water flow of the Mississippi from 45% of the total drainage area. The Ohio River contributes half the water flow of the Mississippi from only 18% of the total drainage area (Meade, 1995, Fig. 5A).

Sediment sources vary even more dramatically, both between and within large river basins. On a global scale, the consistently largest river-sediment loads come from the regions of greatest tectonism. Nearly half the river sediment that reached the coastlines of the world during the 20th century was carried by the large rivers of southern and eastern Asia that drain the tectonic collision zone between the Indian subcontinent and the rest of Asia. Another fourth to a third of the global runoff of river sediment is contributed from the tectonically active islands of the western Pacific region (Milliman and Meade, 1983; Milliman and Syvitski, 1992).

Within many large basins, the same pattern of tectonic control may prevail. Gibbs (1967, p. 1218) estimated that 82% of the total suspended sediment discharged by the Amazon River was supplied by the 12% of the total drainage area that lies in the Andes. More recent publications suggest that 90-95% of the sediment in both the Amazon and Orinoco Rivers is originally derived from the tectonically active area of the Andes (Meade, 1994, Figs. 2-3; 1996, Fig. 1). In some river basins; however, the predominant contributors of sediment may be areas of low tectonism underlain by geologically susceptible materials such as the Quaternary loess deposits in the Yellow River basin or the Mesozoic shales drained by the major western tributaries of the 'Mississippi River.

While variable in space, sediment yields also are variable in time--especially in response to human activities. Sediment discharges in the Yellow River basin increased by an order of magnitude as a result of extensive agricultural development of the loess plateau of northern China that began about 200 BC (Milliman et. al., 1987). Sediment discharges in the Mississippi River have been diminished by more than half, mostly during the last half century, by the construction of dams and other engineering works on the mainstem and its major tributaries (Meade, 1995, Fig. 6A). Other well-known examples of major rivers in which dams and reservoirs have decreased sediment loads are the Indus (Milliman et. al., 1984), Nile (El Dardir, 1994), and Colorado (Meade & Parker, 1985, Fig. 29; Meade, Yuzyk & Day, 1990, Fig. 12).

STORAGE OF SEDIMENT

Understanding the storage and remobilization of sediment in large alluvial systems is an important prerequisite to understanding the fate of sediment-borne contaminants or the construction/destruction of riparian habitats. At seasonal time scales, sediment is stored on the banks and channel beds of all large rivers in response to decreases in water discharge or water-surface slope, and it is remobilized by the next significant increase in discharge or slope. Such seasonal cycles of

storage and remobilization of sediment have been described, for example, in the lower Amazon (Meade et al., 1985, Fig. 2), middle Orinoco (Meade, Weibezahn et al., 1990, p. 72; Meade, 1994, Fig. 7), and lower Mississippi (Meade & Parker, 1985, Fig. 31; Meade, Yuzyk & Day, 1990, Fig. 15) Rivers.

More pertinent to considerations of contaminants and habitats, however, is the storage and remobilization of sediment at longer time scales--centennial, millennial, multimillennial. In the large alluvial plains (llanos) of western Venezuela and eastern Colombia, sands are brought down from the Andes by tributaries of the Orinoco River and deposited into storage where they remain for sufficiently long times that their less stable components, such as lithic fragments, weather out, leaving behind more stable quartz grains to be retransported farther downstream when the deposits are next remobilized by laterally shifting stream channels. This repeated intersection of the long time scale of alluvial storage with that of intense tropical soil weathering results in a progressively maturing assemblage of sand grains in the downstream direction within the Orinoco River system (Johnsson et. al., 1991, Figs. 11-12).

In the middle Amazon River, exchanges between floodplain and channel exceed the downriver flux of sediment. In the 2000-km reach of the Amazon above the last downriver gaging station at Obidos, the average annual increment of sediment added to the tops of the floodplains by overbank deposition is 2.1×10^9 tonnes. The quantity of sediment remobilized from the floodplains back into the river by bank erosion in the same reach during an average year is 1.6×10^9 tonnes (Dunne et. al., 1998, Fig. 10 & Table 3). Both these numbers are larger than the annual downriver flux of sediment past the gage at Obidos, whose measured average is 1.2×10^9 tonnes.

The lowermost reaches of many large river systems seem to be net sinks for sediment. This presumption is difficult to quantify, however, because accurate data on discharges of fresh water and sediment are difficult to collect in river reaches where velocity and stage are affected by fluctuations in ocean tides. The Ob River of Siberia is one of the few large rivers where the topographic configuration allows an effective gaging station to be operated near the mouth. Compared to the quantities measured at the next gaging station 870 km upstream, the amount of fresh water passing the downstream-most gage on Ob River during a 50-yr period (1940-90) was 25% greater than that passing the upstream gage. Meanwhile, the suspended-sediment discharge measured at the downstream gage during the same period was 40% less than the sediment discharge measured at the upstream gage (Bobrovitskaya et al., 1996, Fig. 1; Meade et al., 2000, Fig. 1; Smith & Alsdorf, 1998, Fig. 5). This loss of 40% of the sediment load is most easily explained by deposition on the extensive floodplains that flank the lowermost Ob River.

RIVER SEDIMENT IN COASTAL WATERS

Once in the coastal zone, most river sediment will be deposited in a delta, or estuary, on the proximal continental shelf, or be transported parallel to the shoreline for some distance in the direction of the prevailing coastal current. The proportions of sediment delivered to the different sites of ultimate deposition vary from one river to another. The Yellow River of China deposits

approximately 90% of its sediment in its delta. The combined Ganges and Brahmaputra Rivers deposit about half their sediment in their delta and deliver another quarter or third to be deposited on the proximal continental shelf. The rest of the sediment discharged by the Ganges and Brahmaputra is transported along shore by coastal currents or across the continental shelf to the deep sea where it becomes part of the Bengal submarine fan (Meade, 1996, Fig. 2). Of the Amazon River sediment that passes the last downstream gaging station at Obidos: 30% usually is deposited in the delta or in the floodplains that flank the lowermost river, 50% is deposited on the continental shelf off the river mouth, and 20% is transported northwestward along the northeast coast of South America in large moving mudbanks that eventually reach the outer delta of the Orinoco River (Meade, 1994, Fig. 8).

REFERENCES

Bobrovitskaya, N. N., Zubkova, C. & Meade, R. H. (1996) Discharges and yields of suspended sediment in the Ob' and Yenisey Rivers of Siberia. In: *Erosion and Sediment Yield: Global and Regional Perspectives* (ed. by D. E. Walling & B. W. Webb) (Proc. Exeter Symp., July 1996), 115-123. IAHS Publ. no. 236.

Dunne, T., Mertes, L. A. K., Meade, R. H., Richey, J. E. & Forsberg, B. R. (1998) Exchanges of sediment between the flood plain and channel of the Amazon River in Brazil. *Geol. Soc. America* Bull. 110(4), 450-467.

E I Dardir, M. (1994) Sedimentation in Nile High Dam Reservoir, 1987-1992, and sedimentary futurologic aspects. *Sedimentology of Egypt 2,* 23-39.

Gibbs, R. J. (1967) The geochemistry of the Amazon River system: Part I, The factors that control the salinity and the composition and concentration of the suspended solids. *Geol. Soc. America Bull. 78(10),* 1203-1232.

Johnsson, M. J., Stallard, R. F. & Lundberg, N. (1991) Controls on the composition of fluvial sands from a tropical weathering environment: Sands of the Orinoco River drainage basin, Venezuela and Colombia. *Geol. Soc. America Bull. 103(12),* 1622-1647.

Meade, R. H. (1994) Suspended sediments of the modern Amazon and Orinoco Rivers. *Quaternary Internat. 21,* 29-39.

Meade, R. H. (1995) Setting: Geology, hydrology, sediments, and engineering of the Mississippi River. In: *Contaminants in the Mississippi River, 1987-92* (ed. by R. H. Meade), 13-29. US Geol. Survey Circular 1133.

Meade, R. H. (1996) River-sediment inputs to major deltas. In: *Sea-level Rise and Coastal Subsidence: Causes, Consequences, and Strategies* (ed. by J. D. Milliman & B. U. Haq), 63-85. Kluwer Academic Publishers, Dordrecht.

Meade, R. H., Bobrovitskaya, N. N. & Babkin, V. I. (2000) Suspended-sediment and fresh-water discharges in the Ob and Yenisey Rivers, 1960-88. *International Journal of Earth Sciecnes* 89: 461-469.

Meade, R. H., Dunne, T., Richey, J. IF, Santos, U. de M. & Salati, E. (1985) Storage and remobilization of suspended sediment in the lower Amazon River of Brazil. *Science 228,* 488-490.

Meade, R. H. & Parker, R. S. (1985) Sediment in rivers of the United States. US *Geol. Survey Water-Supply Paper 2275,* 49-60.

Meade, R. H., Weibezahn, F. H., U-.wis, W. M., Jr. & Perez Hernandez, D. (1990) Suspended-sediment budget for the Orinoco River. In: *El Rio Orinoco como Ecosistema* (ed. by F_H. Weibezahn, H. Alvarez & W. M. Lewis Jr.), 55-79. Impresos Rubel, Caracas.

Meade, R. H., Yuzyk, T. R. & Day, T. J. (1990) Movement and storage of sediment in rivers of the United States and Canada. In: *Surfiace Water Hydrology* (ed. by M. G. Wolman & H. C. Riggs), 255-280. *Geol. Soc. America, The Geology of North America* vol. 0-1.

Milliman, J. D. & Meade, R. H. (1983) World-wide delivery of river sediment to the oceans. *J. Geol.* 91(l),1-21.

Milliman, J. D., Qin, Y.-s., Ren, M.-e. & Saito, Y. (1987) Man's influence on the erosion and transport of sediment by Asian rivers: The Yellow River (Huanghe) example. J. *Geol.* 95(6), 751-762.

Milliman, J. D., Quraishee, G. S. & Beg, M. A. A. (1984) Sediment discharge from the Indus River to the ocean: Past, present and future. In: *Marine Geology and Oceanography of Arabian Sea and Coastal Pakistan* (ed. by B. U. Haq & J. D. Milliman), 65-70. Van Nostrand Reinhold, New York.

Milliman, J. D. & Syvitski, J. P. M. (1992) Geornorphic/tectonic control of sediment discharge to the ocean: The importance of small mountainous rivers. J. *Geol. 100(5),* 525-544.

Potter, P. E. (1978) Significance and origin of big rivers. J. *Geol.* 86(l), 13-33.

Potter, P. E. (1998) The Mesozoic and Cenozoic paleodrainage of South America: A natural history. *J. South American Earth Science* 10 (5/6), 331-344.

Smith, L.C. & Alsdorf, D.E. (1998) Control on sediment and organic carbon delivery to the Arctic Ocean revealed with space-borne synthetic aperture radar: Ob River, Siberia. *Geology* 26(5).

ON QUANTIFYING THE EFFECTS OF RIPARIAN VEGETATION IN STABILIZING SINGLE THREADED STREAMS

J. Dungan Smith, Hydrologist, U. S. Geological Survey, Boulder, CO

Abstract: Most natural, single-threaded rivers are sinuous in planiform geometry, and that sinuous morphology typically is maintained by riparian vegetation. Consequently, quantitative evaluation of the potential for a river to resist changing its geometric form from single- to multiple-threaded morphology (unravel) during a severe flood requires reliable algorithms for computation of the resistance of the riparian vegetation to overbank flows of various magnitudes. In this paper a process-based model for computing the erosive properties of overbank flows through woody riparian vegetation is developed and then is tested using data from a severe flood on East Plum Creek (Colorado) in 1965. This flood caused the sparsely and moderately vegetated main stem and tributaries of East Plum Creek to unravel, but the headwater tributaries that were bordered by dense carrs of sandbar willow remained intact. The model predicted these results based on the differing shrub densities.

INTRODUCTION

Urban and rural development in the semi-arid western United States often reduces the density and area of riparian shrubs. This loss of woody vegetation has resulted in a substantial reduction in the ability of the remaining riparian vegetation to reduce the stresses of overbank flows on the flood plain. The result is much greater susceptibility to rapid flood-plain erosion during large floods. Along many perennial montane streams in the western United States, dense carrs of willows intermixed with beaver ponds provided good protection against severe floods in the early 1800's. Many of these carrs have persisted in spite of beaver removal by intense trapping in the first half of the 19th century. Further downstream, the shrub understory of the cottonwood forests similarly protected the banks and the segments of flood plain between bends (flood-plain tabs) from deep overbank flows. Removal of these shrubs increases the vulnerability of the flood plain to erosion. Reliable theoretical procedures to assess the magnitude of this apparent growing flood-plain vulnerability, however, are lacking, and large floods occur infrequently enough and are sufficiently poorly documented when they do occur to make a comprehensive empirical analysis of this issue impossible.

A procedure to calculate flood-plain stability provided by clumps of willow and water birch shrubs of specified density has been developed by the author to assess the vulnerability of the Clark Fork of the Columbia River through the Deer Lodge valley in Montana to catastrophic change in planiform geometry (unraveling). In the case of the Clark Fork, most of the dense carrs of willows and water birch that were present in the early 1900's eventually were killed or drastically thinned by thick deposits (0.1 to 0.6m or more) of metals-contaminated mine tailings contributed during a three-hundred year recurrence interval flood in 1908. Stream stability calculations for the Clark Fork were performed for the reconstructed 1908 flood in the upper Deer Lodge Valley and showed that the 1908 riparian shrub forest was sufficiently dense to prevent the flood plain from unraveling. This protection has now been lost. The model subsequently has been generalized to permit computation of overbank flow and sediment transport characteristics in a wide variety of situations for which the physical properties of the

riparian vegetation are known. In this paper, a version of the general model suitable to analyze flow across flood plains covered by sandbar willow carrs is presented.

To test the computational procedure, it was applied to several headwater tributaries of East Plum Creek after an intense rainfall that lasted for several hours in 1965. This event centered over East Plum Creek and its headwater tributaries. The Plum Creek drainage basin is located just south of Denver, Colorado. Osterkamp and Costa (1987) discuss the geomorphic response of Plum Creek to the associated flood from the confluence of East and West Plum Creeks to its junction with the South Platte River, and Griffin and Smith (this volume) discuss this flood in the main stem of East Plum Creek. In spite of its short duration, the 1965 flood caused the main stems of Plum Creek, East Plum Creek, and some of the more sparsely vegetated headwater tributaries of East Plum Creek to unravel. The flood reduced the sinuosity of these channels from approximately 1.20 to less than 1.05, and it increased the width of the channel by a factor of ten or more.

Sinuous channels can widen by two fluid-mechanically-different processes. These are (1) lateral erosion of banks by the removal of sediment at their bases, which causes under cutting and slumping, and (2) erosion of the flood-plain by deep overbank flows, which begins by rilling and channeling of the flood-plain surface. Kean and Smith address the former issue in this volume; the latter process is the topic of this paper. Aerial photographs taken two days after the 1965 Plum Creek flood demonstrate that the unraveling was accomplished by rapid surface erosion of essentially all of the point bars and the tabs of flood plain behind them as a consequence of the deep overbank flow. Flow and sediment transport calculations based on the aerial photographs indicate that the sand eroded from flood plain tabs quickly filled the original channel and obliterated it, causing the bed of the flood channel to rise in elevation. Subsequent to the initial rapid transformation from a sinuous geomorphic system with bar-pool bed topography to a wide straight one with an approximately uniform rectangular cross section, roughened by upstream-propagating antidunes, the flood channel widened slowly by cut-bank erosion of older terraces. Owing to the short duration of the flood, channel widening by cut-bank erosion of the channel-flanking terraces accounted for only a small fraction of the increase in flood-channel width. Nevertheless, the 1965 flood was the largest one to affect Plum Creek in recent times, and it did cause the channel zone to widen measurably by cut-bank erosion after the flood plain unraveled.

Unlike the situation further downstream where the woody vegetation was less dense and was typically dominated by trees rather than shrubs, the more thickly shrub-vegetated headwater tributaries of East Plum Creek retained their original morphology. At present, the riparian flora of these densely vegetated tributaries is dominated by sandbar willow. The post-flood aerial photographs indicate that a similar willow flora was present at these locations during the flood. In those upstream locations where the tributary channels are now dammed by beaver, the ponds are fringed with sandbar willow, and the aerial photographs indicate that there were beaver ponds in some of these tributaries prior to the flood. During the 1965 flood, most of the beaver dams that bounded distinct ponds were breached locally with cuts that were only a few dam widths across. In contrast, those dams that were back watering willow thickets typically were not breached. Only in a few cases where the beaver ponds were large, the dams were broad, and the willow carrs were thin did the dams wash out and the tributary channels begin to show signs of unraveling. In essence, as long as the riparian shrub flora remained dense, the channel zones remained intact in spite of being subjected to two to three meters of overbank flow.

In the headwater tributaries of East Plum Creek, some of the channels that came unraveled and some of those that remained morphologically intact had essentially the same slope (0.0097 to 0.0107) and were subjected to similar depths of overbank flow (nearly 3m). The discharge in all of these headwater tributaries was huge compared to the flow capacity of the channel. The nature and density of the local riparian shrub vegetation controlled the differences between the responses of these different sites to the fluid-mechanical stresses of the flood. Consequently, after reconstructing the peak discharge during the 1965 flood at these locations, the fluid mechanical and botanical data necessary to test a process-based model could be assembled. Griffin and Smith (this volume) describe the peak-discharge reconstruction. Here the focus is on flood-plain-surface erosion and a model for computation of overbank flow through sandbar willow carrs of different stem densities, as appropriate for the 1965 East Plum Creek flood, is described and tested. For this paper, a depth of 3.00m and a slope of 0.0103 are used.

MODEL FOR COMPUTATION OF DRAG ON RIPARIAN SHRUBS

The flow is assumed to be hydrostatic and unaccelerated. The latter restriction is not essential, but inclusion of accelerations in the equations of motion for the frictionally dominated case of interest here is of no benefit. A formulation analogous to the one presented here can be used to determine the vertical flow structure for quasi-three-dimensional, hydrostatic models, such as the one for flow in curved channels with bed topography of Smith and McLean (1984). It can be used similarly with vertically integrated, numerical flow models such as the one of Wiele et al. (1996).

Sandbar willows bend over when subjected to a deep overbank flow. As a consequence, a multi-layer model is necessary to describe their effect on the flow. The model described in this paper has three layers. The lowest layer extends from $z = z_0$ to $z = z_1$ and is filled with stems that protrude through its upper surface (see sketch to the right). These are modeled as if perpendicular to the flow; that is, the along-stem component of flow induced by their curvature is neglected in the drag calculation. The middle layer extends from z_1 to z_2 and is filled with stems bent parallel to the flow. Skin friction acts on the stems and leaves in this zone and there is form drag on the branches. The third layer extends from z_2 to z_3 and is assumed not to have any drag-producing structural elements in it. If there are drag-producing structures that penetrate the surface of the flow, such as tall trees, then a drag term can be added to the top layer. In addition, if structures of several substantially different sizes and shapes are present, each can be modeled separately by adding additional drag terms. A single term using the average size is sufficient if the drag coefficient does not vary from object to object.

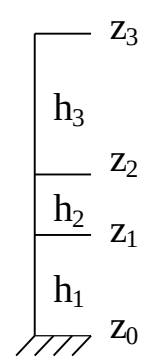

In an unaccelerated, homogeneous-flow situation, the stress divergence balances the downstream component of the fluid weight per unit volume. In the present case, this force per unit volume balance needs to be modified in the bottom and middle layers by subtracting the spatially varying skin friction and drag forces per unit volume on the trees and shrubs. In addition, form drag on the topographic features of the bed needs to be included in the bottom layer, but this is done using the method of Smith and McLean (1977). For a steady, horizontally uniform flow, the force per unit volume balance in the lowest layer reduces to

$$\frac{\partial t_{zx}}{\partial z} = rg(\sin a) + s_D \frac{t_b}{h_1}, \tag{1a}$$

where

$$s_D = \frac{F_D}{l_1^2 h_1 (\frac{t_b}{h_1})} = \frac{C_D}{2k^2}((\ln \frac{h_1}{(z_o)_1}) - 0.74)^2 \frac{h_1 D_S}{l_1^2}. \tag{1b}$$

In (1), τ_{zx} is the shear stress on planes parallel to the average bed of the flow, z is the distance above the average bed, ρ is the density of the fluid, g is the acceleration due to gravity, α is the slope of the bed relative to the horizontal, σ_D is a drag function defined by (1b), $(\tau_{zx})_b = \tau_b$ is the shear stress on the average-bed, h_1 is the thickness of the layer protruded by the trunks of trees and the stems of shrubs, F_D is the drag force on the woody vegetation, λ_1^2 is the mean area affected by a stem, C_D is the drag coefficient for a stem (assumed to be a circular cylinder oriented perpendicular to the flow), k = 0.408 is von Karman's constant, $(z_0)_1$ is the roughness length for the mean bed, and D_S is the mean diameter of the stems causing the drag. Integrating (1a) from z = 0, where $\tau_{zx} = \tau_b$, to $z = z_1$, where $\tau_{zx} = (\tau_{zx})_1$, and solving for τ_b, gives

$$t_b = \frac{(t_{zx})_1 + (-rgh_1(\sin a))}{1 + s_D}. \tag{2}$$

Integrating (1a) from z to z_1, rearranging, and equating τ_{zx} to the shear ($\partial u/\partial z$) using an eddy viscosity (K) yields

$$t_{zx} = (t_{zx})_1 \frac{z}{h_1} + t_b(1 - \frac{z}{h_1}) = rK\frac{\partial u}{\partial z}. \tag{3}$$

For a steady horizontally uniform, channel flow with no drag elements in the interior,

$$K = ku_* z(1 - \frac{z}{h_1}), \quad \text{when } z \le z_m = 0.20h_1 \tag{4a}$$

and

$$K = \frac{ku_* h_1}{ß}, \quad \text{where } \beta = 6.24, \quad \text{when } z \ge z_m = 0.20h_1. \tag{4b}$$

In (4), $u_* = (\tau_b/\rho)^{1/2}$ is the shear velocity. It is the velocity scale for the turbulence in the layer of concern, which in this case is the lowest layer ($z_0 < z \le z_1$). The eddy viscosity profile given by (4) also is used in the middle and upper layers, but in these cases the shear velocities are calculated from the shear stresses at the bases of the appropriate layers ($(u_*)_0 = (\tau_b/\rho)^{1/2}$, $(u_*)_1 = ((\tau_{zx})_1/\rho)^{1/2}$, $(u_*)_2 = ((\tau_{zx})_2/\rho)^{1/2}$). For the flow situation considered in this paper, the scales of the turbulent transfer of momentum are modified by the presence of woody vegetation. Consequently, (4a) is used throughout the lower layer and (4b) is used throughout the middle and upper layers. The appropriate length scales in each of the layers are the layer thicknesses.

Substituting (4a) with $u_* = (u_*)_0$ into (3) and integrating from $z = z_0$ to $z \le z_1$ gives for $z_0 \le z \le z_1$

$$u = \frac{(u_*)_0}{k}((\ln\frac{z}{z_o}) + \frac{(t_{zx})_1}{t_b}(\ln\frac{(1-z_0/h_1)}{(1-z/h_1)})) = \frac{u_*}{k}((\ln\frac{x}{x_o}) + \frac{(t_{zx})_1}{t_b}(\ln\frac{(1-x_0)}{(1-x)})) \quad (5)$$

where $\xi = z/h_1$ and $\xi_0 = z_0/h_1$.

Similarly, substituting (4b) with $u_* = (u_*)_1$ into an equation analogous to (3), but for the second layer, and integrating from $z_1 = \xi_1 h_1$ to $z \le z_1 = \xi_1 h_1$ gives for $z_1 \le z \le z_2$

$$u = \frac{(u_*)_1}{k}ß\left(\left((x - \frac{1}{2}?^2) - (x_1 - \frac{1}{2}x_1^2)\right) + \frac{(t_{zx})_2}{t_b}\left(\frac{x^2 - x_1^2}{2}\right)\right) + \quad (6)$$

$$\frac{(u_*)_1}{k}\left(\left(\ln\frac{?_1}{?_0}\right) + \frac{(t_{zx})_2}{t_b}\left(\ln\frac{(1-?_0)}{(1-?_1)}\right)\right).$$

In the upper-most layer of thickness h_3, there is no drag force, so

$$\frac{\partial t_{zx}}{\partial z} = rg(\sin a), \quad (7)$$

$$(t_{zx})_2 = -rgh_3(\sin a), \quad (8)$$

and

$$t_{zx} = (t_{zx})_2(1 - \frac{(z - z_2)}{h_3}) = rK\frac{\partial u}{\partial z}, \quad (9)$$

The velocity field for this upper layer can be calculated from (4b) and (9). It is as given by (6), with $(\tau_{zx})_1 = 0$, $(u_*)_1$ replaced by $(u_*)_2$, and z replaced by $z-z_2$. The effective roughness length $(z_0)_2$ for this layer is increased substantially relative to $(z_0)_1$ because of the low velocity zones within and beneath the layer of horizontal stems.

The middle layer supports a substantial shear across it when the number of sandbar willow stems is large. This layer is assumed to thin as the spacing between shrubs increases. The equation of motion for the middle layer is

$$\frac{\partial t_{zx}}{\partial z} = rg(\sin a) + s_{DB}\frac{(t_{zx})_1}{h_2} + s_{SF}\frac{(t_{zx})_1}{h_2}, \quad (10a)$$

where

$$s_{DB} = \frac{C_D}{2k^2}((\ln\frac{h_2}{(z_o)_1}) - 1)^2\frac{h_2 D_B}{l_2^2} \quad (10b)$$

and

$$s_{SF} = \frac{C_{SF}}{2k^2}((\ln\frac{h_2}{(z_o)_1}) - 1)^2 (N_S p \frac{D_S}{l_2} + N_L \frac{wl}{A_c}) . \qquad (10c)$$

In (9), $\sigma_{DB}((\tau_{zx})_1/h_2)$ represents the drag on the branches, which have a mean diameter of D_B and affect a volume of $h_2\lambda_2^2$. In addition, $\sigma_{SF}((\tau_{zx})_1/h_2)$ represents the skin friction stress on the downstream-oriented stems of circumference πD_S and length $H_{SF} = \gamma_{HSF}D_S$ and on the leaves of mean width w and length l. The number of overlapping stems per λ_2 in the middle layer is N_S, and the number of leaves in the canopy of a clump of sandbar willows is N_L. Here N_L is estimated as $2A_C/A_L$ where A_L is the area of one leaf. The area of the flood plain affected by that canopy of area A_C is denoted A_{FP}; therefore, the canopy density is A_C/A_{FP}. The roughness length for the flow in this zone of thickness h_2 is $(z_0)_2$. The skin-friction coefficient (C_{SF}) in (9c) is $1.328R_L^{-1/2}$, where $R_L = UL/\nu$ is the Reynolds number for the viscous boundary layer on a stem or leaf of length L. Here, (U) the velocity at the edge of the boundary layer, estimated as the average velocity of the layer, and ν is the kinematic viscosity of the water. Calculations show that skin friction on the stems and leaves is several orders of magnitude smaller than the drag on the branches: therefore, an accurate estimate of the number of leaves in the canopy of a clump of sandbar willows is not essential.

If the trees and shrubs do not bend over, as in the case with many types of willows that are associated with active and extant beaver ponds in the Northern Rocky Mountains, then only one layer need be considered. This is the situation on the flood plain of the Clark Fork through the Deer Lodge Valley, which is dominantly populated with bebbs, geyer, and yellow willows and with water birch (Paul Hansen, personal communication). For this case, the equations for the bottom layer can be used by themselves; they need be modified only by setting $(\tau_{zx})_1$ to zero, letting h_1 be the total depth, and accounting for the change in cross-sectional area with distance above the bed (caused by the decrease in stem diameter and the increase in number of branches).

APPLICATION OF MODEL TO THE 1965 FLOOD ON EAST PLUM CREEK

In the headwater tributaries of East Plum Creek, the stems of the larger sandbar willows range from 0.01 to 0.04m in diameter (D) and average about 0.03m in diameter (D_S). They are about H = 100D tall. In a shallow flow, depth (h) < 0.5m, these shrubs protrude through the surface, but in a deep flow, such as occurred in 1965 (2.0 < h < 3.0m), they bend over like grass, forming a surface beneath which the shear stresses are very low. These willows apparently have evolved a flexible stem that permits them to survive very high flow velocities by preventing erosion of the surface into which they are rooted. At a given locality, all of the stems bend to a nearly uniform surface set by their average size, because there is much more drag on the tops of those shrubs that would ordinarily bend on a larger radius and protrude above this plane. Similarly, there is much less drag on the tops of those stems that would ordinarily bend on a smaller radius. The measured bending radius using a spring scale is about 20D, so this stem layer averages about $20D_S$ above the flood plain surface. The mean thickness of the bent-over-stem layer is about half of its height ($10D_S$). The zone of stems, branches and leaves acts as a moving, hydraulically rough bed for the high-flow region above ($z > 25D_S$) and a low velocity layer forms in the region below ($z < 15D_S$).

To obtain the characteristic geometric parameters of the shrubs necessary for the analysis presented in this paper, measurements were made in healthy sandbar willow carrs in the upper East Plum Creek drainage. These carrs appeared typical of ones in the same areas that did not unravel in the 1965 flood according to the aerial photographs taken right after the flood. A willow shrub consists of a clump of stems connected below the surface. At these sites the typical stem spacing (D_L) in a clump is $4D_S$ and the clump (group) diameter is about $D_G = \gamma_G D_S = 20D_S$. Therefore, $D_L = \gamma_L D_S = 4D_S$. The stem clumps ($D_C$) are somewhat less than $2D_G = 40D_S$ apart. The canopies in a clump are tightly intermingled and the canopies of the stem clumps also are intermingled. Sandbar willows are typically tall and thin with their branches primarily near the top of the shrub. As a consequence, the bending moment on them is high and, when dense, they extend several clump diameters in the streamwise direction, evening out the tendency to group and forming what is modeled as a thick but uniform and nearly planar zone about $10D_S$ in vertical extent (the middle layer).

The sediment bed beneath the shrubs can be modeled as having irregularities with a length scale comparable to the average distance between stems ($4D_S$) and a depth of the average stem diameter (D_S). There also is topography with a wavelength set by the spacing between clumps ($D_C \approx 40\ D_S$) and a height of $2D_S$. At least to a first approximation, each of the pertinent lengths appears to scale by the average stem diameter (D_S), reducing the complexity of the set of pertinent input parameters. The pertinent scaling ratios for the calculations presented in this paper are $\gamma_L = D_L/D_S$, $\gamma_G = D_G/D_S$, and $\gamma_C = D_C/D_G$. The values of these ratios for the dense canopy case described above are 4, 20, and 2 respectively.

DISCUSSION

Results of calculations for the 1965 flood in the East Plum Creek tributaries are summarized in Table 1. The dense riparian shrub vegetation produced a large amount of drag that resisted the 1965 flood in these tributaries. This can be seen by comparing the boundary shear stresses listed in Table 1 to $\rho gh(\sin\alpha) = 303 N/m^2$, the boundary shear stress that would result if there were no

Table 1: Results of calculations for East Plum Creek tributaries.
[The absence of information or lack of resolution is indicated by --]

Mean non-dimensional distance between stems	6	8	10	12	16	20	24	32	40	80
Vertically averaged flow velocity (m/s)	2.17	2.34	2.63	2.90	3.37	3.83	4.27	5.05	5.70	7.80
Flow velocity in lower layer (m/s)	0.230	0.297	0.471	0.638	0.979	1.34	1.69	2.35	2.91	4.78
Shear stress on top of bottom layer (N/m^2)	1.54	4.93	12.6	22.4	46.4	72.9	98.5	141	172	232
Boundary shear stress on the average bed (N/m^2)	0.222	0.582	1.40	2.50	5.72	10.4	16.1	29.5	43.7	105
Boundary shear stress on the actual surface (N/m^2)	0.039	0.130	0.370	0.752	2.08	4.32	7.45	15.8	25.8	78.0
Unraveling predicted ($\tau_b > (\tau_b)_{cr}$)	NO	NO	NO	NO	--	YES	YES	YES	YES	YES
Unraveling occurred	NO	NO	NO	--	--	--	YES	YES	YES	YES

form drag producing elements in the flow. This table also shows that the effectiveness of shrubs in reducing boundary shear stresses produced by deep overbank flows drops off rapidly with increasing stem spacing. In the three cases with the most dense shrub vegetation, the actual boundary shear stresses were well below the critical shear stress for erosion of the slightly cohesive, sparse-grass-covered, sandy soil into which the sandbar willows were rooted ($(\tau_b)_{cr} \approx 2$ N/m^2).

As shown in Table1, the drag model calculations employing no empirical adjustments agree with the observed extent of flood-plain erosion and provide a good first estimate of the fluid mechanical effects of woody vegetation on a flood plain subjected to a large flood. A process-based model of this type has the advantage of permitting calculations for flood plains that are conceptually deforested to various degrees in order to evaluate the damage that could occur under these scenarios. In the case of the Plum Creek Flood of 1965, the model provided good discrimination between those reaches that were predicted to remain geomorphologically intact and those that had insufficiently dense woody riparian vegetation to prevent unraveling.

SUMMARY AND CONCLUSIONS

Boundary shear stresses were computed for flows through sandbar willow carrs of densities estimated for several upstream tributaries of East Plum Creek during the 1965 flood. These calculations indicate that the drag on the shrubs in the densest carrs reduced the boundary shear stresses to below the value required to erode the slightly cohesive, sandy soil beneath the shrubs. In all these cases, the canopies of the individual willow clumps were intertwined. In contrast, in those cases where the non-dimensional stem spacing dropped below 16 along the margins of the stream, the shrub density was insufficient to prevent rapid erosion of the thin grass sod between the clumps of shrubs, and all these areas unraveled. Short beaver dams in areas with intermingled canopies along the stream banks and on the flood-plain tabs were breached locally, but the rest of the dams provided enough form drag in combination with that on the near-by-riparian vegetation to prevent geomorphic degradation of the riparian corridor. Only in the cases of sequences of large beaver ponds with long dams and sparse lateral vegetation did the dams wash out. The overbank flow model was able to handle each of these situations correctly; therefore, it can be concluded that the model provides a useful tool for investigating the vulnerability of sparsely vegetated flood plains to floods of various magnitudes.

REFERENCES

Griffin, E.R., and J.D. Smith, This Volume, Computation of bankfull and flood-generated hydraulic geometries in East Plum Creek, Colorado.

Kean, J.W. and J.D. Smith, This Volume, Computation of Sediment Erosion from the Base of Cut Banks in River Bends.

Osterkamp, W.R. and J.E. Costa, 1987, Changes accompanying an extraordinary flood on a sand-bedded stream, in Catastrophic Flooding, ed. by L. Mayer and D. Nash, Allen and Unwin, Boston, 201-223.

Smith, J.D. and S.R. McLean, 1977, Spatially averaged flow over a wavy surface, Journal of Geophysical Research, 82(12), 1735-1746.

Smith, J.D. and S.R. McLean, 1984, A model for flow in meandering streams, Water Resources Research 20( ), 1301-1315.

FLOODS AND GEOMORPHIC CHANGE IN THE SOUTHWESTERN UNITED STATES: AN HISTORICAL PERSPECTIVE

Robert H. Webb, Hydrologist, U.S. Geological Survey, 1675 W. Anklam Road, Tucson, AZ; Richard Hereford, Geologist, U.S. Geological Survey, 2255 N. Gemini Drive, Flagstaff, AZ

Abstract: Arroyos are channels incised into their former floodplains. In the arid and semiarid parts of the Southwest, most arroyos formed between 1862–1909, causing severe agricultural and infrastructure damage. Arroyo cutting and re-filling have occurred episodically in the late Holocene throughout the region. After about 1940, many arroyos in the region partly aggraded and developed floodplains. Many causes have been proposed for arroyo cutting, particularly the introduction of livestock, climatic change (particularly drought), intrinsic geomorphic response, and combinations of these factors. Climatic fluctuations that changed regional flood frequency offer the most parsimonious explanation for arroyo cutting. A series of large floods that occurred in discrete periods between 18621–942 are responsible for arroyo incision in the Southwest; a resurgence in flooding between 1964–1993 renewed channel erosion in southern Arizona (with the notable exception of the San Pedro River) and the southern Colorado Plateau as well. The occurrence of these floods was highly influenced over the short term by El Niño - Southern Oscillation (ENSO) conditions, which in turn were influenced by decadal-scale climatic fluctuations. The dynamic channels of arroyos have prompted extensive flood-control and channel-stabilization efforts that continue to the present.

INTRODUCTION

Arroyo cutting, the downcutting and widening of vertical-walled channels by ephemeralstreams, caused numerous environmental and economic problems in the American Southwest around the turn of the century. Between 1862–1909, almost all of the alluvial channels in the region became incised deeply into their floodplains (Table 1). Arroyo cutting caused large economic losses, including destruction of agricultural lands and irrigation networks. Although geomorphologists have extensively researched the reasons for arroyo cutting, large disagreements persist in their conclusions (compare Hereford, 1986; Webb and Baker, 1987; Graf, 1983; Elliott et al., 1999).

In this paper, we briefly review the circumstances surrounding the formation of arroyos, noting in particular the association of historical arroyo cutting with periods of extreme regional floods. The wide distribution of arroyo cutting suggests a regional cause for an essentially synchronous (in geologic terms) hydrologic event. Because arroyos have formed and re-filled several times in the late Holocene, any overall explanation for arroyo behavior must take into account factors other than 19th century land uses. We also note that the legacy of channel change set in motion at the end of the 19th century continues to affect floodplain management in the region.

ARROYO CUTTING: THE LATE HOLOCENE

Much of the disagreement about the cause for arroyo cutting and filling hinges on whether arroyos cut and fill "synchronously." The word "synchronous" has come to mean "exactly the same time" or "within an interval defined by dating error," depending upon who is using the term. Most geologists consider deposition to be synchronous if discrete packages of sediment can

Table 1. Dates for initiation of arroyo cutting in 25 tributaries of the Colorado River (from Bryan, 1925; Graf, 1983; Webb, 1985; Hereford, 1993; Hereford et al., 1996).

Stream or River	State/Drainage	Incision Date	Cessation of Erosion
Pack and Mill Creeks	UT/Colorado	1896	1919
Bull Creek	UT/Fremont	1932	1935
Fremont River	UT/Colorado	1896	1909
Escalante River	UT/Colorado	1909	1932
Walker Creek	AZ/San Juan	1880	1894
Montezuma Creek	UT/San Juan	1880s	n.d.
San Juan River	UT/Colorado	1884	1911
Paria River	UT/Colorado	1884	1909
Rio de Flag	AZ/Colorado	1890-1892	n.d.
Little Colorado River	AZ/Colorado	1880	1940
Kanab Creek	UT-AZ/Colorado	1882	1909
Santa Clara River	UT/Virgin	1862	1889
Virgin River	UT/Colorado	1862-1883	1909
Mangas River	NM/Gila	1881-1891	n.d.
Silver City Wash	NM/Gila	1887	1892
San Simon River	AZ/Gila	1883	1891
Blue River	AZ/Gila	1900-1906	1920
San Pedro River	AZ/Gila	1883	1908
Arivaca Creek	AZ/San Pedro	1863	1917
Sonoita Creek	AZ/Santa Cruz	1891	n.d.
Pantano Wash	AZ/Santa Cruz	1890s	n.d.
Rillito Creek	AZ/Santa Cruz	1872	1891
Santa Cruz River	AZ/Gila	1878	1891
Gila River	AZ/Gila	1880	1891
Whitewater Draw	AZ/Whitewater	1884	n.d.

be mapped regionally and placed into one time period. Some hydrologists consider synchroneity to refer to simultaneous occurrence, as if every downcutting event occurred at exactly the same moment. The latter definition is unrealistic, given the nature of the geologic information.

Numerous studies have addressed the timing of late Holocene cutting and re-filling in arroyo systems (e.g., Hereford et al., 1996). Elliott et al. (1999) summarize selected radiocarbon dates, focusing mostly on arroyos in New Mexico. They noted a wide spread in dates of arroyo cutting and concluded that each basin has a unique alluvial history. Because alluvial stratigraphy is dated with either radiocarbon, archaeological remains, or dendrochronology, synchroneity can only be discussed in relatively broad (sub-century or longer) time spans, not with the accuracy expected by Elliott et al. (1999).

For southern Utah, the dates of arroyo cutting and filling during the last thousand years are relatively well known and are reasonably synchronous in geologic terms (Fig. 1). From before AD 1000 to about AD 1200, channels in southern Utah were filled with sediment, in many cases well higher than the levels of historical floodplains. Between about AD 1200–1400, downcutting occurred. Afterwards, these channels filled rapidly, in some cases in less time than can be

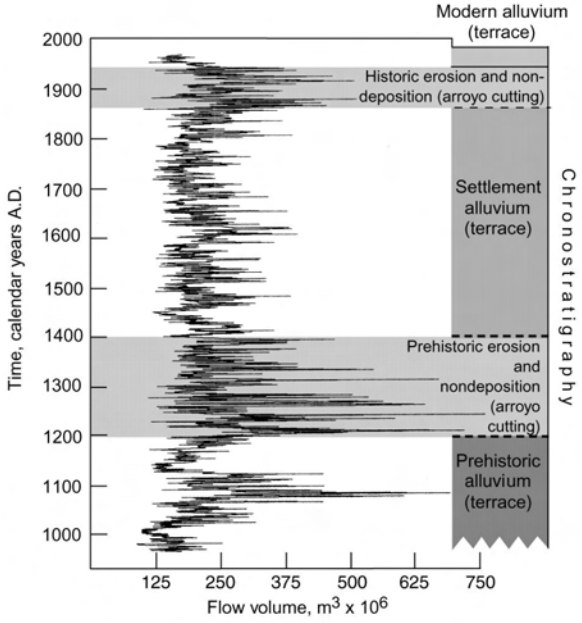

Figure 1. Generalized alluvial chronostratigraphy of the southern Utah – northern Arizona region compared with a dendrochronological reconstruction of annual flow volumes of the Virgin River from AD 966-1965. The dendrochronological reconstruction is modified from Larson and Michaelsen (1990, fig. 9). The late Holocene alluvial chronostratigraphy is from Hereford et al. (1996) and Euler et al. (1979). Heavy and light dashed lines indicate regional variation of < 50–100 years and < 25–50 years, respectively, in dating of erosion and subsequent alluviation. The two erosional episodes are temporally associated with increased runoff and absence of regional alluviation.

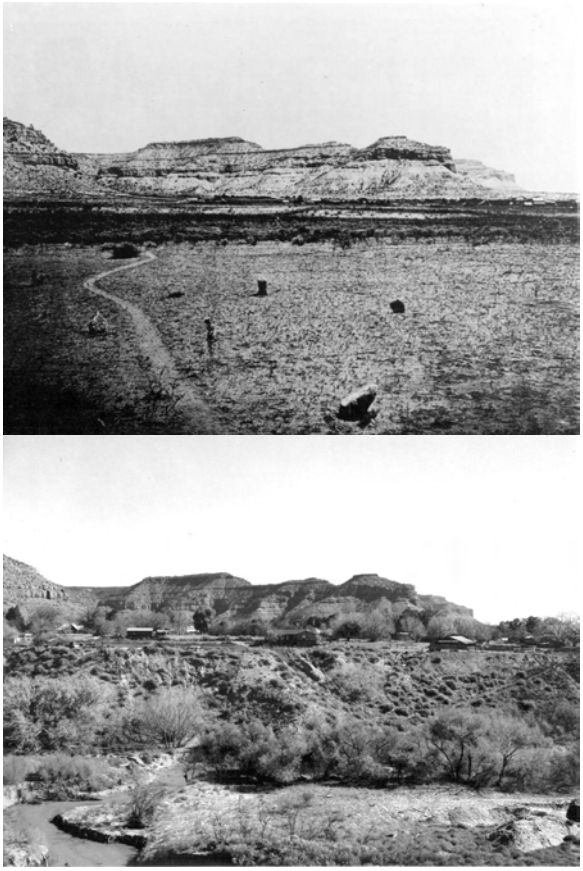

Figure 2. Effects of arroyo cutting on Kanab Creek, Kanab, Utah.

A. (1872). In 1872, Kanab Creek was shallowly incised (~1 m depth) into a broad floodplain. The dominant riparian species in this view is the native coyote willow. Floods between 1882–1909 cut a deep channel through the floodplain, causing severe agricultural and water supply damages (photograph by J.K. Hillers, from Dutton, 1882).

B. (1990). In 1990, the arroyo of Kanab Creek was about 30 m deep and 100 m wide. The current depth was reached after the 1909 flood. Development of a floodplain within the arroyo walls has created riparian habitat, and native and non-native trees are thriving in this perennial reach (Robert H. Webb).

resolved using radiocarbon dating (Webb and Hasbargen, 1998), and general aggradation occurred between about AD 1400–1860. As discussed in the next section, arroyos in the region once again downcut after settlement of the region.

ARROYO CUTTING: THE HISTORICAL PROBLEM

Before about 1860–1890, most alluvial channels in the Southwest were shallowly incised into floodplains (Figure 2A). Geologic evidence and historical reports suggest that overbank flooding was common, and this combined with high groundwater levels sustained riparian ecosystems. Beginning in 1862, and particularly in the decade 1880–1890, arroyo cutting began throughout the Southwest, particularly in the Colorado River drainage (Table 1). All arroyos did not entrench in exactly the same years (Webb, 1985; Webb and Baker 1987, and Elliott et al., (1999), and most active channel erosion ceased after about 1942 (Hereford, 1986) and in some cases much earlier. In fact, most historical arroyos in the Southwest began and completed downcutting between about 1880–1932 (Table 1).

ARROYO CUTTING: SOME CAUSAL MECHANISMS

The cause of arroyo cutting is one of the most studied problems in the geomorphology of the Southwest (see Graf, 1983; Webb, 1985). For historical arroyos, many scientists, particularly those trained as conservationists or land managers, cite overgrazing as the primary cause, largely because runoff and sediment yield are increased from trampled, denuded land. Others, particularly those with geological training link arroyo cutting to climatic variation. More complicated explanations invoke livestock overgrazing as the triggering device for climatically induced historical downcutting. Some researchers call upon the spatial variability of sediment transport in ephemeral streams, leading to the concept of "intrinsic geomorphic response." Still others find an association of unusually large floods and climatic fluctuations with arroyo incision. Cooke and Reeves (1976), in an insightful observation, stated that the "—final conclusion from this brief comparison is perhaps the simplest and most obvious: apparently similar arroyos can be formed in different areas as a result of different combinations of initial conditions and environmental changes." Although the admonition is well taken, the search for "the cause" for arroyos continues.

Domestic Livestock and Human Impacts.

Livestock overgrazing in the late 19th century was so pervasive on some ranges that denudation was severe, particularly during the drought of 1891-1896 when half of the cattle in the region are believed to have perished. The scientific argument implicating livestock grazing holds that the hooves of livestock compact soil, increasing runoff and sediment yield. Cattle trails through riparian thickets channelize flow, focusing erosive energy on the floodplain. Agricultural development and road construction are also cited as mechanisms for focusing erosion, and indeed many arroyos developed along historical roads.

The problem with livestock as the only cause for arroyo formation lies in several inconsistencies among the introduction of livestock, their environmental effects, and channel downcutting. Grazing could not have caused prehistoric arroyo cutting (Fig. 1) because livestock were not on

the landscape. Livestock were introduced to the Southwest in the 1700s (Hastings and Turner, 1965), well before historic arroyo cutting began. Some arroyos formed almost immediately after settlement (Table 1), which is not enough time for overgrazing to significantly affect the landscape. Moreover, the effects of grazing are at odds with increased axial valley erosion. Runoff and hillslope erosion are greatly increased in overgrazed areas, but the extra sediment delivered to floodplains should enhance deposition, not create more erosion. For these reasons, some researchers have turned to regional causes such as intrinsic geomorphic processes and climatic change instead of attributing arroyo cutting to only poor land-use practices.

Intrinsic Geomorphic Processes.

The concept of intrinsic geomorphic processes began with Schumm and Hadley (1957) and it was further elaborated by Patton and Schumm (1981). According to this notion, incised channels were formed and re-filled owing to the special character of sediment-transport and erosional processes in semiarid climates. The high sediment yields typical of this climate are thought to oversteepen stream gradients, which in turn drives cycles of arroyo cutting and filling. Arroyo systems are thought to have reaches of predominantly erosion, where knickpoint retreat causes channel incision, and reaches of predominantly aggradation, where sediment eroded from upstream reaches is deposited. Under this concept, climate does not play a major role in arroyo development, and livestock are thought to have triggered the sediment-transport processes leading to arroyo cutting that would have occurred even without grazing.

Intrinsic geomorphic processes are appealing because the concept explains the apparent lack of synchroneity in arroyo cutting and filling (Patton and Schumm, 1981). This mechanism also directly incorporates poor land-use practices, such as livestock grazing, to increase sediment yields. However, this concept does not consider that many channel systems developed axial arroyos through nearly the entire length of their alluvial valleys. Also, the concept requires asynchronous cutting and filling cycles; however, the late Holocene chronostratigraphy (Fig. 1) and historical overlap in downcutting (Table 1) could not have occurred from intrinsic geomorphic processes alone. As a result, this mechanism offers a model for the short-term movement of sediment through ephemeral channel systems, but it neither predicts adequately the timing of arroyo cutting and filling nor explains the drainage-wide scale of historical downcutting.

Climatic Forcing: Drought.

During the 1890s, protracted drought occurred in the Southwest, leading to large livestock and agricultural losses. Some arroyos downcut during this period, suggesting that drought was associated with and caused by arroyo cutting (Bryan, 1925; Euler et al., 1979). Drought alone is unlikely to cause channel erosion for the obvious reason that water must be in the channel for sediment to be transported, so researchers sought to link drought to watershed changes that would make hillslopes more susceptible to erosion. These changes include a weakening of grass cover by drought and (or) grazing and decreased density of riparian vegetation and channel roughness owing to decreased ground-water levels in the alluvial aquifer. During ensuing runoff, flood waters, swelled by low vegetation cover on hillslopes, encountered less flow resistance, and floodplain deposits not bound by plant roots were quickly eroded.

Figure 3. Annual flood series for rivers in southern Arizona.

A. San Francisco River near Clifton, Arizona. B. Santa Cruz River near Tucson, Arizona.

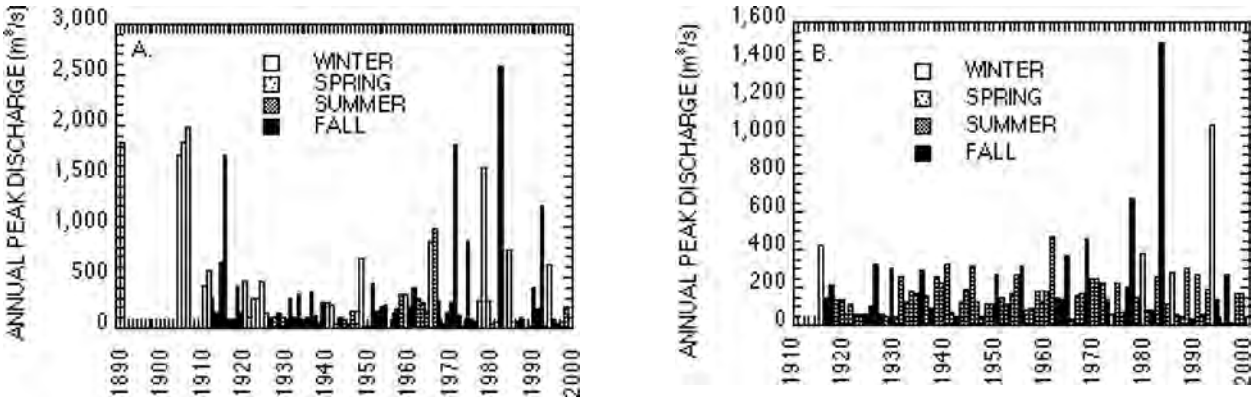

Drought may have influenced arroyo formation in some areas, but it did not cause arroyo cutting in southern Utah. In Upper Valley Creek, the relation between ground-water levels and arroyo initiation is not consistent through the late Holocene (Webb and Hasbargen, 1998). In particular, water levels were highest just before the arroyo downcut. Gregory and Moore (1931) report that flow in Upper Valley Creek increased 4-fold after 1882, suggesting that ground-water levels were high just before arroyos became incised in the region; dendrochronological reconstructions of streamflow in the Virgin River support this anecdotal information (Fig. 1). Webb (1985) noted that downcutting in southern Utah spanned 50 years and did not correlate well with years of high or low annual precipitation (as recorded in tree-ring or instrumental records). Lack of close association reduces the possibility that drought-induced lowering of alluvial aquifers was fundamental to arroyo incision.

Climatic Forcing: Floods.

Arroyos for which historical documentation is available began downcutting during floods. The question is how big were the floods and were they related to regional climatic variation? Many researchers associate large floods with the initiation of arroyos (Graf, 1983). Webb and Baker (1987), for example, found that periods of arroyo formation were associated with large floods on the Escalante River of southern Utah. The floods most responsible for arroyo cutting had recurrence intervals greater than 100 years, depending upon the period over which flood frequency was calculated. Webb et al. (1991) discuss the cause of arroyo formation on Kanab Creek in southern Utah and note the extreme flood damage reported in historical accounts, as originally discussed by William Morris Davis in 1903. Hereford et al. (1996) found a similar association on the upper Virgin River.

Our understanding of changes in flood frequency before the turn of the century is hampered by relatively short gaging records, which in this region mostly begin in the 1920s. Paleoflood studies (e.g., Webb and Baker, 1987) suggest that the floods that initiated arroyos were considerably larger than those recorded in mid-20th century gaging records. The discharges of some of these floods approach the envelope curve of the largest floods recorded on the Colorado Plateau (Webb, 1985). Gaging records that have historical peaks, such as the San Francisco River near Clifton, Arizona, support this conclusion (Fig. 3a). In this case, the 1891 flood is the

largest in the historical record and larger than most 20th century floods until 1983. For this record and others in the region, including the Santa Cruz River at Tucson, Arizona (Fig. 3b), flood frequency increased again after about 1960, but this change was delayed in southern Utah and northern Arizona until the late 1970s to early 1980s.

Flood frequency and streamflow in the Southwest are highly influenced by global-scale climatic processes, particularly El Niño – Southern Oscillation (ENSO; Webb and Betancourt, 1992; Cayan and Webb, 1993). ENSO conditions have a periodicity of 4-7 years and result from relatively well-understood processes in the equatorial Pacific Ocean as well as concomitant changes in extratropical circulation patterns in the upper atmosphere. ENSO effects vary geographically in a predictable pattern known as climatic teleconnections; the Southwest, particularly Arizona, has increased flood frequency during warm ENSO conditions (El Niño), and the Pacific Northwest has increased flood frequency during cool (La Niña) conditions. The forcings for decadal-scale climatic fluctuations are poorly understood, but they are probably significant geomorphically owing to the influence of repeated flooding compared with isolated floods. Decadal-scale climatic fluctuations influence most of the western United States, although in any given year flooding may occur in one part of the region and drought in another. This aspect of climatic forcing explains why large floods – and the arroyo cutting they cause – do not occur "synchronously" in the region.

Decadal-scale climatic fluctuations provide a reasonable explanation for late Holocene arroyo formation in the Southwest. Floods – particularly regional events that affect many river systems – have a much higher probability of occurrence during warm ENSO conditions, although floods do not occur in all such years (La Niña conditions more reliably produce droughts). El Niño particularly influences the type and seasonality of floods. Flood frequency was particularly high between 1880–1909 in the Southwest; flood frequency again increased between the mid-1960s–1995 (Fig. 3). The geomorphic effect of this latter increase was not apparent until the late 1970s to early 1980s, when most channels eroded the former floodplain producing the modern terrace. These changes are linked to global-scale fluctuations in decadal climate; warm ENSO conditions during some decades are more effective at producing channel-changing floods than during other decades. Therefore, hydroclimatology, as it affects flood frequency and channel morphology, is an important factor in assessing channel stability as well as for planning of floodplain structures.

CONCLUSIONS

In historical time, arroyos in the Southwest formed during a period of unusually large floods between 1862–1942, with most of the erosion occurring between 1880–1909. Flooding is related to global-scale climatic variability and offers the most viable explanation for both historical arroyo cutting as well as prehistoric downcutting in the late Holocene. The spatial variability of climatically driven changes in flood frequency accounts for the lack of "synchroneity" in arroyo processes.

REFERENCES

Bryan, K., 1925, Date of channel trenching (arroyo cutting) in the arid Southwest. Sci. 62, 338-344.

Cayan, D.R., Webb, R.H., 1992, El Niño/Southern Oscillation and streamflow in the western United States, *in*, Diaz, H.F., Markgraf, V., (*eds.*), El Niño, historical and paleoclimatic aspects of the southern oscillation. Cambridge Univ. Press, 29-68.

Cooke, R.U., Reeves, R.W., 1976, Arroyos and environmental change in the American South-West. London, Oxford Univ. Press, 213 p.

Dutton, C.E., 1882, The Tertiary history of the Grand Canyon district. U.S. Geol. Sur. Mono. 2, 228-229.

Elliott, J.G., Gellis, A.C., Aby, S.B., 1999, Evolution of arroyos: incised channels of the southwestern United States., *in*, Darby, S.E., and Simon, A., (*eds.*), Incised river channels. New York, John Wiley, p. 154-183.

Euler, R.C., Gumerman, G.J., Karlstrom, T.N.V., Dean, J.S., Hevly, R.H., 1979, The Colorado Plateaus: Cultural dynamics and paleoenvironment. Sci. 205, 1089-1101.

Graf, W.L., 1983, The arroyo problem, paleohydrology and paleohydraulics in the short term, *in* Gregory, K.J., *ed*., Paleohydrology. New York, John Wiley, 279-302.

Gregory, H.E., Moore, R.C., 1931, The Kaiparowits Region, a geographic and geologic reconnaissance of parts of Utah and Arizona. U.S. Geol. Sur. Prof. Paper 164, 161 p.

Hastings, J.R., Turner, R.M., 1965, The changing mile. Tucson, Univ. Ariz. Press, 317 p.

Hereford, R., 1986, Modern alluvial history of Paria River drainage basin, southern Utah. Quat. Res. 25, 293-311.

Hereford, R., 1993, Entrenchment and widening of the upper San Pedro River, Arizona. Geol. Soc. Amer. Special Paper 282, 46 p.

Hereford, R., Jacoby, G.C., McCord, V.A.S., 1996, Late Holocene alluvial geomorphology of the Virgin River in the Zion National Park area, southwest Utah. Geol. Soc. Amer. Special Paper 310, 41 p.

Larson, D.O., Michaelsen, J., 1990, Impacts of climatic variability and population growth on Virgin Anasazi developments. Amer. Antiq. 55, 227-249.

Patton, P.C., Schumm, S.A., 1981, Ephemeral-stream processes: Implications for studies of Quaternary valley fills. Quat. Res. 15, 24-43.

Schumm, S.A., Hadley, R.F., 1957, Arroyos and the semiarid cycle of erosion. Amer. Jour. Sci. 255, 161-174.

Webb, R.H., 1985, Late Holocene flooding on the Escalante River, south-central Utah [Ph.D disser.]. Tucson, Univ. Ariz., 204 p.

Webb, R.H., Baker, V.R., 1987, Changes in hydrologic conditions related to large floods on the Escalante River, south-central Utah, *in* Singh, V., *ed*., Regional flood-frequency analysis. Dordrect, The Netherlands, D. Reidel, 306-320.

Webb, R.H., Smith, S.S., McCord, V.A.S., 1991, Historic channel change of Kanab Creek, southern Utah and northern Arizona. Grand Canyon Nat. History Assoc. Mono. 9, 91 p.

Webb, R.H., Betancourt, J.L., 1992, Climatic variability and flood frequency of the Santa Cruz River, Pima County, Arizona. U.S. Geol. Sur. Water-Supply Paper 2379, 40 p.

Webb, R.H., Hasbargen, J., 1998, Floods, groundwater levels, and arroyo formation on the Escalante River, south-central Utah, *in* Learning from the Land. Proc. Grand Staircase - Escalante National Monument, November 1-5, 1995, 49-59.

Author contact—Robert H. Webb, U.S. Geological Survey, 1675 W. Anklam Rd., Tucson, AZ 85745, rhwebb@usgs.gov; Richard Hereford, U.S. Geological Survey, 2255 N. Gemini Dr., Flagstaff, AZ 86001, rhereford@usgs.gov.